Supplementary information

Oxime-based 19-Nortestosterone-Pheophorbide *a* Conjugate: Bimodal Controlled Release Concept for PDT

Vladimíra Pavlíčková[1], Michal Jurášek[2], Silvie Rimpelová[1]*, Kamil Záruba[3], David Sedlák[4], Markéta Šimková[2,5], David Kodr[2], Eliška Staňková[2], Jan Fähnrich[3], Zdeňka Rottnerová[6], Petr Bartůněk[4], Oldřich Lapčík[2,5], Pavel Drašar[2]* and Tomáš Ruml[1]*

[1]*Department of Biochemistry and Microbiology, University of Chemistry and Technology Prague, Technická 5, 166 28, Prague 6, Czech Republic*

[2]*Department of Chemistry of Natural Compounds, University of Chemistry and Technology Prague, Technická 5, 166 28, Prague 6, Czech Republic*

[3]*Department of Analytical Chemistry, University of Chemistry and Technology Prague, Technická 5, 166 28, Prague 6, Czech Republic*

[4]*CZ-OPENSCREEN: National Infrastructure for Chemical Biology, Institute of Molecular Genetics AS CR Prague, CZ-142 20 Prague, Czech Republic*

[5]*Institute of Endocrinology; Národní 8, 116 94, Prague 1, Czech Republic*

[6]*Central Laboratories, University of Chemistry and Technology Prague, Technická 5, 166 28, Prague 6, Czech Republic*

Corresponding authors:

Silvie Rimpelová, e-mail: silvie.rimpelova@vscht.cz

Pavel Drašar, e-mail: pavel.drasar@vscht.cz

Tomáš Ruml, e-mail: tomas.ruml@vscht.cz

Table of content

1. Chemistry

1.1. General methods and materials

19-Nortestosterone was purchased from Sigma-Aldrich, azidoPEG$_3$-amine from Click chemistry tools Bioconjugate Technology Company and pheophorbide *a* from Frontier Scientific. These chemicals were used without further purification. Other common chemicals were purchased from Sigma-Aldrich. Solvents were redistilled prior to use.

NMR Spectra (^{1}H and ^{13}C) were recorded by Varian Gemini 300 (^{1}H 300 MHz and ^{13}C 75 MHz). Chemical shifts are given in δ (ppm). HRMS was measured by Micro Q-TOF with ESI ionization. FTIR spectra were measured by Nicolet iS10 model using ATR technique (KBr crystal). Plates coated with silica gel by Stahl (10-40 μm, Merck) and aluminum TLC sheets for detection in UV light (TLC Silica gel 60 $F_{254,}$ Merck) were used for thin-layer chromatography. For visualization, diluted solution of sulfuric acid in MeOH was used and plates were successively heated. For column chromatography, silica gel (30-60 μm, SiliTech, MP Biomedicals) was used.

1.2. Synthesis

(17β)-17-{[*Tert*-butyl(dimethyl)silyl]oxy}estr-4-en-3-one[1] (**P-1**)

This derivative was prepared according to the procedure found in the literature[1]. 19-Nortestosterone (100 mg, 0.36 mmol), *tert*-butyldimethylsilyl chloride (82 mg, 5.47 mmol), imidazole (49 mg, 0.72 mmol) were stirred overnight in 1,4-dioxane (5 mL). Then, the mixture was diluted with ether and washed with bicarbonate solution and water and dried over $MgSO_4$ and the solvent was evaporated. The residue was chromatographed in hexane-EtOAc (10/1→5/1) to obtain the product (123 mg, 0.32 mmol) in 87% yield. R_F=0.64 in hexane-EtOAc 5:1, a slightly pink spot. ^{1}H NMR (300 MHz, $CDCl_3$) δ ppm: -0.01 (d, *J*=2.1 Hz, 6 H, 2×C*H*$_3$), 0.74 (s, 3 H, 18-C*H*$_3$), 0.86 (s, 9 H, 3×C*H*$_3$), 0.88 - 1.08 (m, 6 H), 1.16 - 1.63 (m, 8 H), 1.70 - 1.96 (m, 5 H) 2.00 - 2.14 (m, 1 H), 2.16 - 2.50 (m, 5 H), 3.55 (t, *J*=8.2 Hz, 1 H, 17-C*H*), 5.80 (t, *J*=2.1 Hz, 1 H); Fig. S8. ^{13}C NMR (75 MHz, $CDCl_3$) δ ppm: 11.30, 18.06, 23.29, 25.81, 26.18, 26.58, 30.70, 30.78, 35.50, 36.51, 36.76, 40.47, 42.58, 43.29, 49.32, 49.71, 81.55, 124.46, 166.91, 199.98. IR cm^{-1}: 3305 (*vw*), 2950 (*vs*), 2932 (*vs*), 2856 (*m*), 2735 (*vw*), 2706 (*vw*), 2650 (*vw*), 1667 (*vs*), 1614 (*m*), 1469 (*w*), 1450 (*w*), 1415 (*w*), 1387 (*w*), 1361 (*w*), 1332 (*w*), 1250 (*m*), 1257 (*m*), 1209 (*w*), 1139 (*w*), 1084 (*m*). HRMS ESI: *monoisotopic mass:* 388.27976 Da, found *m/z* 389.28735 (clcd 389.28703) corresponds to [M+H], 411.26938 (clcd 411.26898) for [M+Na] and 427.24316 (clcd 427.24292) for [M+K] ion of the proposed structure; Fig. S1.

({[(17β)-17-{[*Tert*-butyl(dimethyl)silyl]oxy}estr-4-en-3-ylidene]amino}oxy)acetic acid (**P-2**)

Compound **1** (100 mg, 0.26 mmol) and *O*-(carboxymethyl)hydroxyamine hemihydrochloride (37 mg, 0.33 mmol) were dissolved in dry MeOH (5 mL). Then, pyridine (100 μL) was added and the mixture was stirred for 7 h, after which toluene (10 mL) was added and the solvent was removed under reduced pressure. The residue was chromatographed (EtOAc) to obtain product **2** (101 mg, 0.22 mmol) in 84% yield. R_F= 0.2 in EtOAc, a greenish spot. ^{1}H NMR (300 MHz, $CDCl_3$) δ ppm: -0.01 (d, *J*=1.76 Hz, 6 H, 2×C*H*$_3$), 0.73 (s, 3 H, 18-C*H*$_3$), 0.87 (s, 9 H, 3×C*H*$_3$), 0.92 - 2.27 (m, 16 H), 2.30 - 2.51 (m, 1 H), 3.03 (dd, *J*=13.0, 4.5 Hz, 1 H), 3.55 (t, *J*=8.2 Hz, 1 H, 17-C*H*), 4.60 (d, *J*=1.8 Hz, 2 H, CMOC*H*$_2$), 5.84 (s, 0.6 H, C=C*H*), 6.49 (s, 0.4 H, C=C*H*), 9.50 (br. s., COO*H*); Fig. S8.^{13}C NMR (75 MHz, $CDCl_3$) δ ppm: -4.85, -4.52, 11.30, 18.07, 21.77, 23.33, 25.68, 25.82, 26.08, 26.28, 26.94, 27.10, 30.81, 31.00, 35.22, 35.74, 36.84, 36.89, 40.58, 40.67, 41.95, 43.15, 43.31, 49.38, 49.44, 49.68, 49.95, 69.78, 69.88, 81.63, 81.68, 111.52, 117.18, 153.19, 156.07, 157.11, 158.99, 174.70. IR cm^{-1}: 2952 (*vs*), 2927 (*vs*), 2857 (*s*), 2737 (*vw*), 2649 (*vw*), 2560 (*vw*), 1732 (*m*), 1632 (*w*), 1470 (*w*), 1448 (*w*), 1432 (*w*), 1406 (*w*), 1361 (*w*), 1250 (*m*), 1212 (*w*), 1138 (*m*), 1097 (*vs*), 1026 (*m-w*), 857 (*m*), 835 (*m*), 775 (*m*). HRMS ESI: *monoisotopic mass*: 461.28516 Da, found *m/z* 462.30330 (clcd 462.60641) corresponds to [M+H], 484.28516 (clcd 484.28536) to [M+Na] and 500.25901 (clcd 500.25929) to [M+K] ion of the proposed structure; Fig. S2.

N-(2-{2-[2-(2-Azidoethoxy)ethoxy]ethoxy}ethyl)-2-({[(17β)-17-{[*tert*-butyl(dimethyl)silyl]oxy}estr-4-en-3-ylidene]amino}oxy)acetamide (**P-3**)

Compound **2** (70 mg, 0.15 mmol) and aminoPEG$_3$-azide (46 mg, 0.21 mmol) were dissolved in dry CH_2Cl_2 (3 mL) and EDC (33 mg, 0.21 mmol), DMAP (17 mg, 0.21 mmol) and HOBt (0.15 mmol, 21 mg) were added. The mixture was stirred at RT for 4 h. The solvent was evaporated under reduced pressure and the residue was chromatographed ($CHCl_3$-MeOH, 50/1). Azido-derivative **3** (93 mg, 0.14 mmol) was obtained in 94% yield. ^{1}H NMR (300 MHz, $CDCl_3$) δ ppm: -0.01 (d, *J*=1.8 Hz, 6 H, 2×C*H*$_3$), 0.73 (s, 3 H, 18-C*H*$_3$), 0.86 (s, 9 H, 3×C*H*$_3$), 0.88 - 1.08 (m, 4 H), 1.13 - 1.62 (m, 7 H), 1.68 - 2.27 (m, 10 H), 2.29 - 2.50 (m, 1 H), 3.37 (t, *J*=4.98 Hz, 2 H, PEGC*H*$_2$), 3.47 - 3.53 (m, 2 H, PEGC*H*$_2$), 3.51 - 3.58 (m, 3 H, PEGC*H*$_2$ & 17-C*H*), 3.60 - 3.69 (m, 10 H, 4×PEGC*H*$_2$), 4.49 (d, *J*=2.3 Hz, 2 H, CMOC*H*$_2$), 5.82 (s, 0.5 H, C=C*H*), 6.45 (s, 0.5 H, C=C*H*), 6.58 - 6.71 (m, 1 H, N*H*); Fig. S8. ^{13}C NMR (75 MHz, $CDCl_3$) δ ppm: -4.87, -4.54, 11.29, 18.04, 21.79, 23.30, 25.76, 25.80, 26.05, 26.28, 27.04, 27.16, 30.77, 31.04, 35.17, 35.78, 36.81, 36.86, 38.62, 38.67, 40.54, 40.64, 41.92, 43.16, 43.28, 43.30, 49.35, 49.41, 49.70, 49.98, 50.60, 69.80, 69.85, 70.05, 70.26, 70.56, 70.58, 70.65, 72.60, 72.74, 76.57, 77.42, 81.59, 81.64, 111.31, 117.24, 152.78, 155.68, 156.92, 158.51, 170.04, 170.21. IR cm^{-1}: 3431 (*w*), 3349 (*w*),

2951 (*vs*), 2927 (*vs*), 2859 (*vs*), 2103 (*s*), 1677 (*s*), 1632 (*m*), 1530 (*m*), 1470 (*m*), 1450 (*m*), 1360 (*w*), 1343 (*w*), 1285 (*m*), 1251 (*m*), 1136 (*vs*), 1084 (*vs*), 1014 (*w*). HRMS-ESI: *monoisotopic mass*: 661.42346 Da, found *m/z* 662.43130 (clcd 662.43074) corresponds to [M+H], 684.41330 (clcd 684.41268) for [M+Na] and 700.40712 (clcd 700.38662) for [M+K] ion of the proposed structure; Fig. S3.

N-(2-{2-[2-(2-Aminoethoxy)ethoxy]ethoxy}ethyl)-2-({[(17β)-17-{[*tert*-butyl(dimethyl)silyl]oxy}estr-4-en-3-ylidene]amino}oxy)acetamide (**P-4**)

Azido-derivative **P-3** (70 mg, 0.11 mmol) and triphenylphosphine (58 mg, 0.22 mmol) were dissolved in THF (5 mL) and the mixture was refluxed for 3 h, after which water (150 μL) was added. Reduction was continued overnight, after which the solvent was evaporated and the product was chromatographed ($CHCl_3$-MeOH, 50/1→10/1) to obtain amino-derivative **4** (60 mg, 0.09 mmol) in 89% yield. ^{1}H NMR (300 MHz, $CDCl_3$) δ ppm: -0.02 (s, 6 H, 2×C*H*$_3$), 0.73 (s, 3 H, 18-C*H*$_3$), 0.85 (s, 9 H, 3×C*H*$_3$), 0.91 - 2.27 (m, 20 H), 2.30 - 2.62 (m, 1 H), 2.79 - 3.07 (m, 2 H), 3.41 - 3.77 (m, 16 H, PEGC*H*$_2$), 4.49 (s, 2 H, CMOC*H*$_2$), 5.81 (s, 0.5 H, C=C*H*), 6.45 (s, 0.5 H, C=C*H*), 6.68 - 6.92 (m, 1 H, N*H*); Fig. S8. ^{13}C NMR (75 MHz, $CDCl_3$) δ ppm: -4.87, -4.54, 11.28, 18.04, 21.79, 23.29, 25.76, 25.79, 26.05, 26.28, 27.03, 27.16, 30.76, 31.03, 35.17, 35.77, 36.79, 36.85, 38.65, 38.68, 40.53, 40.63, 41.58, 41.91, 43.15, 43.27, 43.29, 49.34, 49.40, 49.69, 49.97, 69.83, 69.88, 70.17, 70.23, 70.45, 70.46, 70.48, 72.58, 72.72, 73.05, 81.57, 81.62, 111.34, 117.26, 152.72, 155.63, 156.86, 158.48, 170.08, 170.25. IR cm^{-1}: 3426 (*m*), 3355 (*m*), 3306 (*m*), 2951 (*vs*), 2923 (*vs*), 2859 (*vs*), 2738 (*vw*), 2710 (*vw*), 2661 (*vw*), 1665 (*s*), 1632 (*m*), 1533 (*m*), 1470 (*m*), 1433 (*m*), 1387 (*w*), 1360 (*w*), 1286 (*w*), 1250 (*m*), 1136 (*vs*), 1085 (*vs*), 1015 (*m*). HRMS ESI: *monoisotopic mass* 635.43296 Da, found *m/z* 636.44034 (clcd 636.44024) corresponds to [M+H], 658.42189 (clcd 658.42218) for [M+Na] and 674.39552 (clcd 674.39612) for [M+K] ion of the proposed structure; Fig. S4.

Nortestosterone-pheophorbide *a* conjugate (**NT-Pb*a***)

Compound **P-4** (50 mg, 0.08 mmol) and Pb*a* (56 mg, 0.09 mmol) were dissolved in dry THF (2 mL) and HOBt (12 mg, 0.09 mmol), DIPEA (16 mg, 0.12 mmol) and DIC (15 mg, 0.12 mmol) were added. The mixture was stirred for 12 h at RT, after which the mixture was diluted with EtOAc and washed with potassium bisulfate (2×30 mL), water (1×30 mL), brine (1×30 mL) and dried over $MgSO_4$. The solvents were removed and the residue was redissolved in MeOH (2 mL). Then, AcCl (660 μL) was added dropwise and the mixture was stirred at RT for 4 h. Thereafter, the heating was removed and crushed ice was added. The product was extracted with EtOAc (5×30 mL) and combined organic layers were washed with sodium bicarbonate solution (2×30 mL), water

(2×30 mL) and dried over $MgSO_4$. The solvent was removed under reduced pressure and the crude product was repetitively chromatographed ($CHCl_3$-MeOH, 100/1→20/1) to give pure product (44 mg, 0.04 mmol) in 51% yield. R_F= 0.25 in CH_2Cl_2-MeOH 20:1, a greenish spot. ^{1}H NMR (300 MHz, $CDCl_3$) δ ppm: -1.70 (s, 1 H, pheoN*H*), 0.02 - 0.24 (m, 1 H), 0.27 - 0.52 (m, 3 H), 0.56 (s, 3 H, 18-CH_3), 0.63 - 1.57 (m, 12 H), 1.63 (t, *J*=7.6 Hz, 3 H, pheoCH_3), 1.81 (d, *J*=6.7 Hz, 3 H, pheoCH_3), 1.85 - 2.49 (m, 8 H), 3.12 (s, 3 H, pheoCH_3), 3.17 - 3.41 (m, 18 H, PEGCH_2 & pheoCH_2) 3.50 - 3.63 (m, 6 H, pheoCH_3 & C*H*-17 & pheo CH_2), 3.88 (s, 3 H, pheoCOOCH_3), 4.20 (d, *J*=5.6 Hz, 1 H, N*H*), 4.45 (d, *J*=4.1 Hz, 2 H, CMOCH_2), 4.47 - 4.55 (m, 1 H, pheoC*H*), 5.63 (s, 0.5 H, C=C*H*), 6.09 - 6.21 (m, 2 H, allylCH_2), 6.24 - 6.34 (m, 1.5 H, pheoC*H* & C=C*H*), 6.48 - 6.74 (m, 1 H), 7.89 (dd, *J*=17.6, 11.7 Hz, 1 H, pheoC*H*), 8.48 - 8.58 (m, 1 H, pheoC*H*), 9.20 - 9.28 (m, 1 H, pheoC*H*), 9.34 - 9.43 (m, 1 H, pheoC*H*); Fig. S8.^{13}C NMR (75 MHz, $CDCl_3$) δ ppm: 11.06, 11.38, 12.31, 12.34, 17.64, 19.56, 21.86, 23.13, 23.38, 25.69, 25.93, 26.12, 27.05, 27.28, 30.34, 30.62, 30.82, 33.38, 35.10, 35.73, 36.28, 36.33, 38.80, 38.85, 39.32, 40.33, 40.45, 41.76, 42.86, 43.09, 49.34, 49.50, 49.56, 49.68, 50.42, 51.64, 53.16, 65.01, 69.84, 69.89, 69.92, 70.16, 70.18, 70.24, 70.49, 70.52, 72.82, 72.83, 72.94, 81.52, 81.61, 93.48, 97.62, 104.49, 105.48, 111.48, 117.30, 123.07, 129.11, 129.14, 129.16, 132.17, 136.34, 136.40, 136.45, 136.69, 138.03, 142.26, 145.35, 149.84, 152.60, 155.81, 156.79, 158.58, 161.72, 164.89, 170.02, 170.32, 170.53, 172.48, 172.93, 189.89. IR cm^{-1}: 3425 (*m*), 3390 (*m*), 3086 (*w*), 2951 (*s*), 2923 (*s*), 2866 (*s*), 2242 (*w*), 1736 (*s*), 1665 (*vs*), 1619 (*s*), 1579 (*w*), 1539 (*s*), 1499 (*m*), 1435 (*m*), 1450 (*m*), 1410 (*m*), 1346 (*m*), 1295 (*m*), 1245 (*m*), 1221 (*m-s*), 1123 (*s*), 1093 (*s*), 1034 (*m*), 986 (*m*), 911 (*m*). HRMS ESI: *monoisotopic mass* 1095.60449 Da, found *m/z* 1118.59455 (clcd 1118.59371) corresponds to [M+Na] ion of the proposed structure; Fig. S5&S6. HPLC: Fig S7.

1.3. Mass spectra, HPLC, NMR

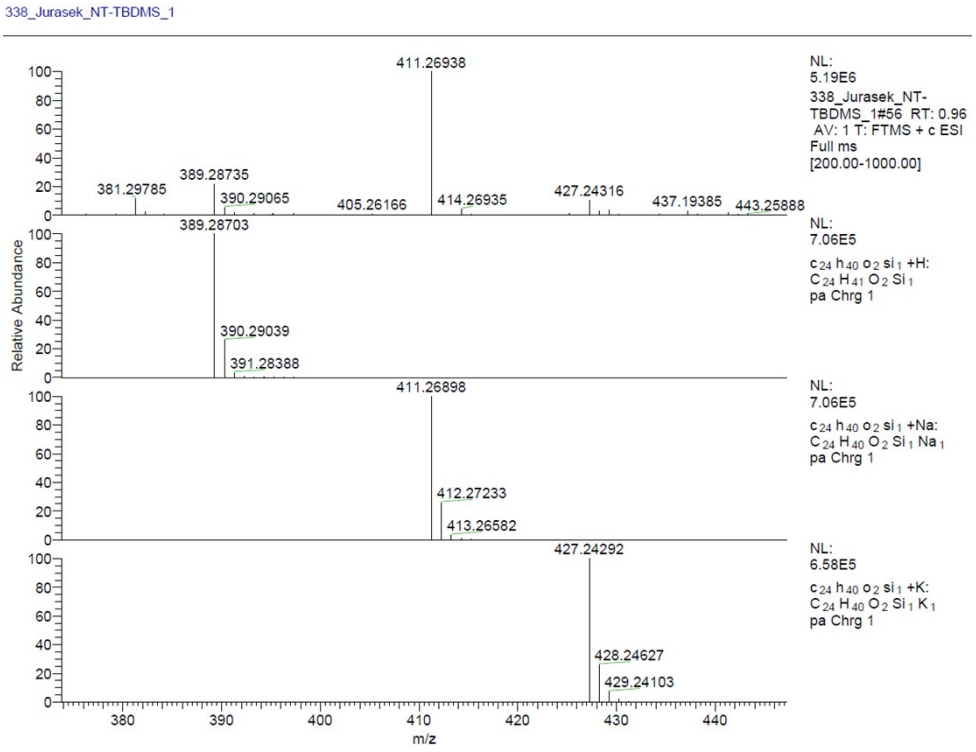

Fig. S1: HRMS spectrum of **P-1**.

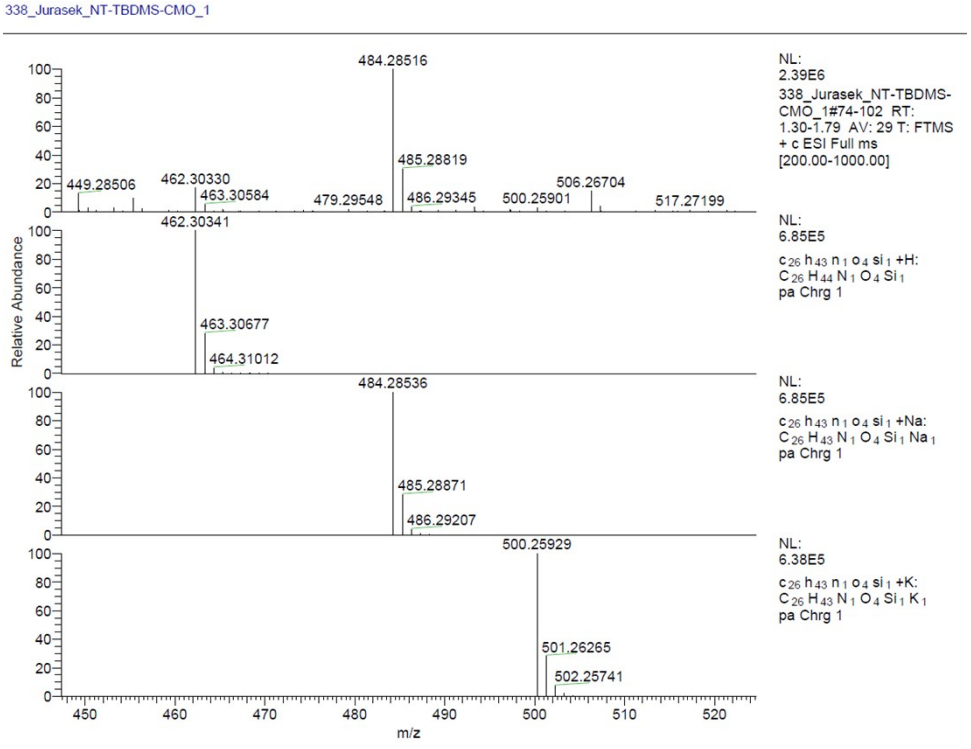

Fig. S2: HRMS spectrum of **P-2**.

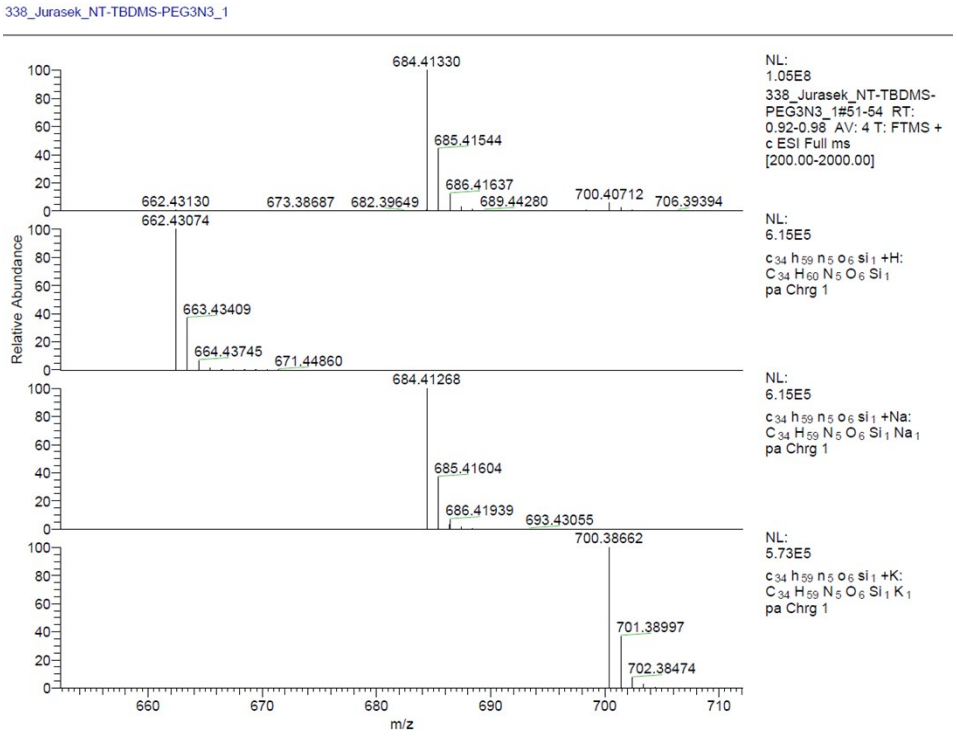

Fig. S3: HRMS spectrum of **P-3**.

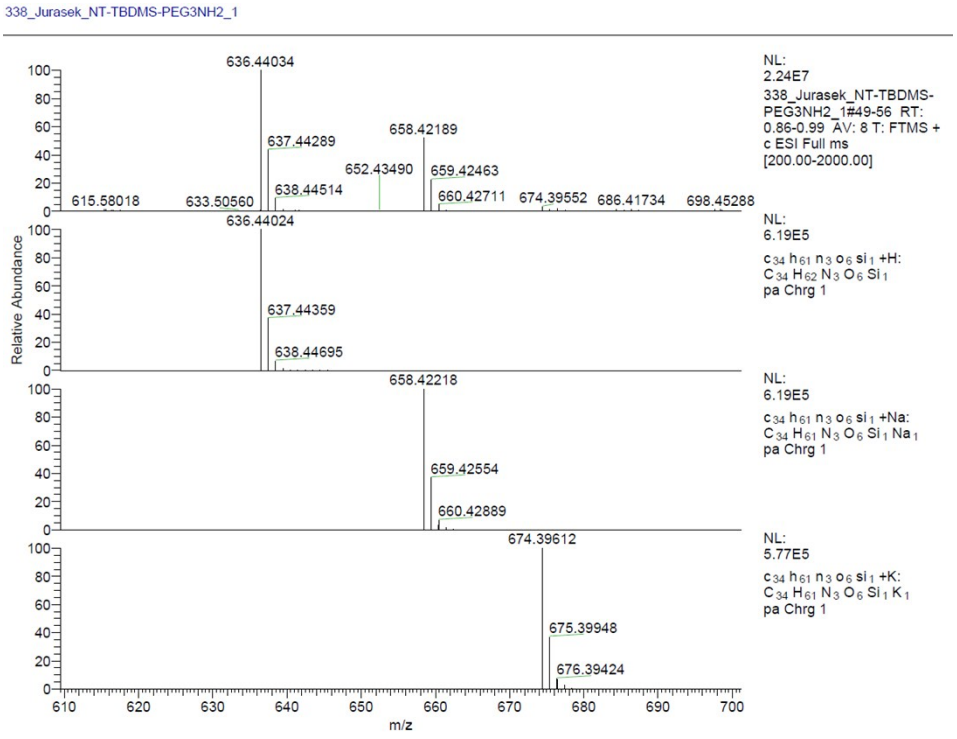

Fig. S4: HRMS spectrum of **P-4**.

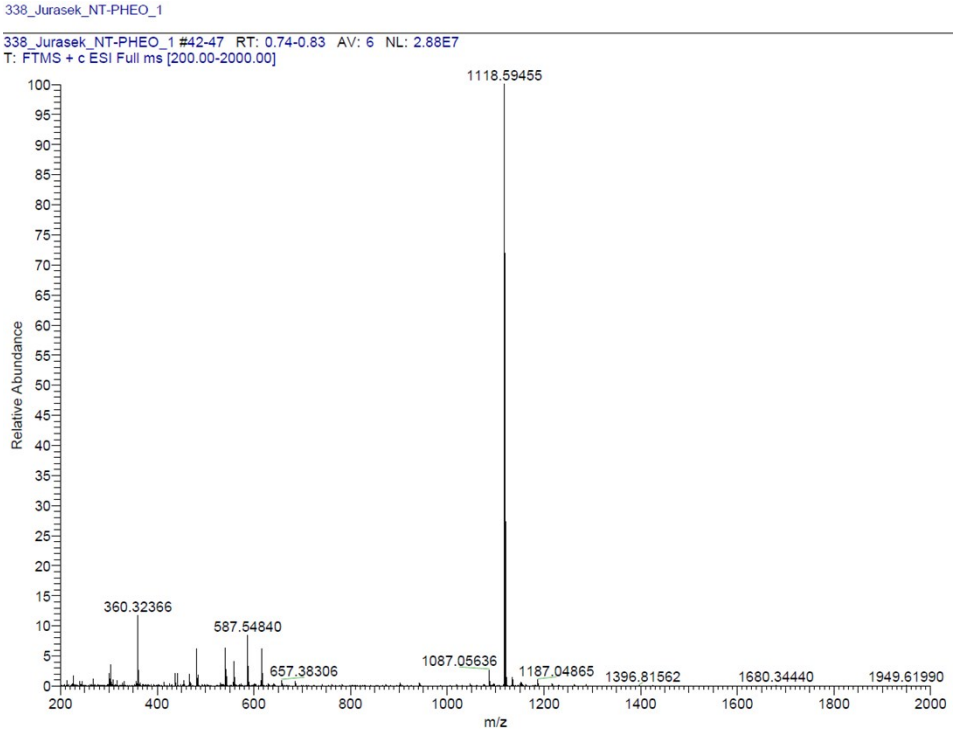

Fig. S5: HRMS spectrum (full scan) of **NT-Pb*a***.

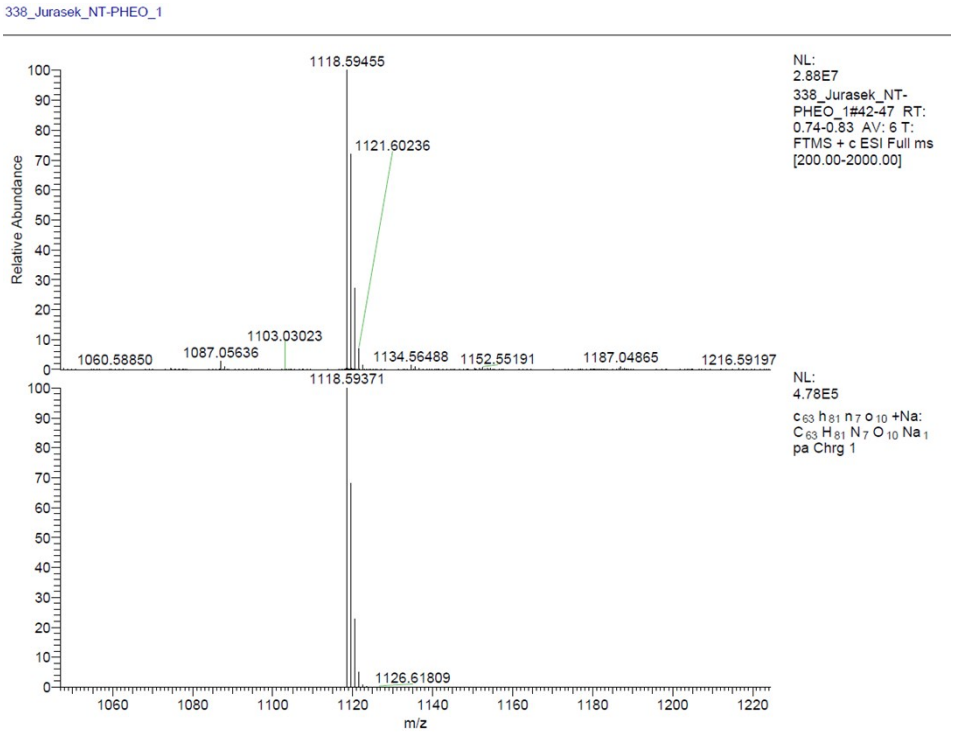

Fig. S6: HRMS spectrum of **NT-Pb*a***, a detail.

HPLC of NT-Pb*a*

Column Luna C18 100 × 4.6 mm, 3 µm; 5 – 100 B in 5 min, 100 % C in 10 min, method 20 min, A = 25 mM NH_4HCO_3, B = 50% AcCN + NH_4HCO_3, C = AcCN. Chromatogram detection with 410 nm.

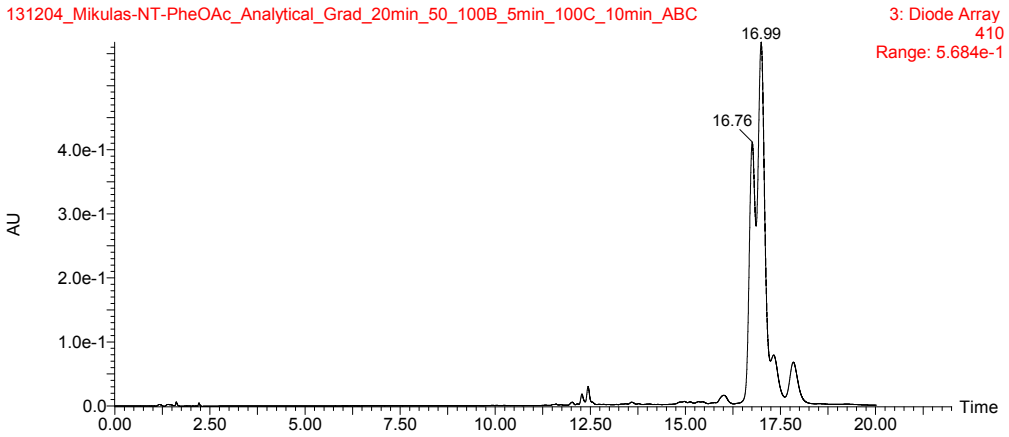

Fig. S7: HPLC of NT-Pb*a*. The chromatogram shows two major *Z/E* isomers (RT 16.76 and 16.99) of the proposed structure. The two peaks behind (RT 17.32 and 17.18 min.) have the same mass suggesting slow equilibrium establishment on C18 column.

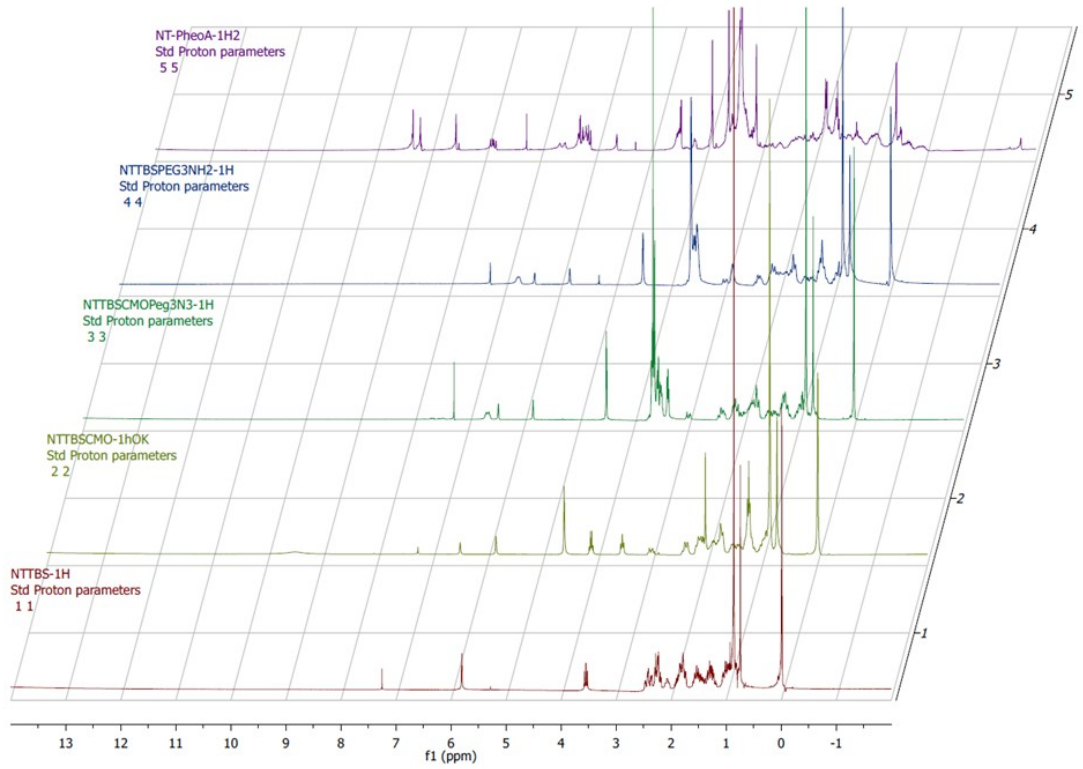

Fig. S8: NMR Spectra of compound **P-1** (1, red line), **P-2** (2, light green line), **P-3 (**3, deep green line), **P-4** (4, blue line) and of **NT-Pb*a*** (5, violet line).

2. Indirect spectrophotometric measurement of singlet oxygen production

2.1. Data measurement

Single oxygen production by photosensitizers Pb*a* and NT-Pb*a* conjugate in Dulbecco's Modified Eagle Medium with 10% fetal bovine serum (DMEM+FBS) was evaluated using uric acid (UA) as a species reactive with singlet oxygen. Rose Bengal (RB) was used as a reference photosensitizer. A stock solution of RB was prepared in water. Stock solutions of Pb*a* and NT-Pb*a* were prepared by dissolving a solid in MeOH. Working solutions were prepared by diluting the stock solutions with air saturated solvent which was either phosphate buffered saline (PBS, pH 7.4) or DMEM+FBS. Concentrations of the working solutions were $c_{RB0} = 1.34 \cdot 10^{5}$ M, $c_{ph0} = 7.76 \cdot 10^{-5}$ M, $c_{ph\text{-}nn0} = 2.01 \cdot 10^{-4}$ M). A stock solution of UA was prepared by dissolving the solid substance in PBS or DMEM+FBS ($c_{ua0} = 8.33 \cdot 10^{-4}$ M). Four different amounts of the photosensitizer (20–75 µL of stock solution) and 100 µL of UA stock solution were mixed with 1 mL of solvent in a plastic cuvette (1.000 cm, PMMA, Kartell, Italy). Two replicates of the same photosensitizer concentration were prepared. The first was kept in the dark, the second was illuminated with a 150 W halogen lamp with an edge-pass filter (Panchromar, Germany) that transmitted light at wavelengths > 500 nm. The fluency rate at the cuvette containing solution was 5 $mW \cdot cm^{-2}$. Relative emission intensity of the source was measured using spectrofluorometer Fluoromax 2 (Horiba Scientific). The lamp illuminated a plate made of barium sulfate positioned on the front surface accessory of the spectrofluorometer and spectrum was recorded (Fig. S9).

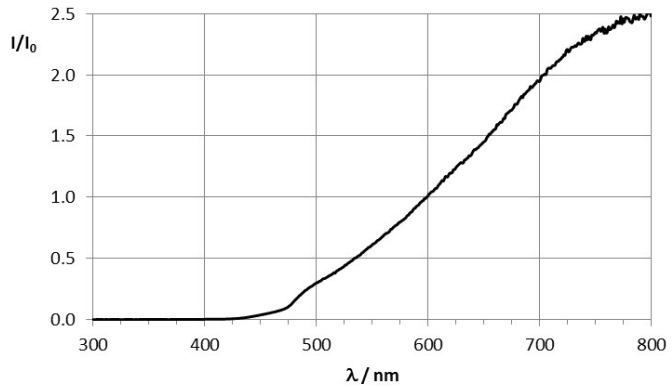

Fig. S9: Spectrum of source relative emission intensity

Emission correction function supplied by manufacturer was applied to the measured spectra. The same correction factor was used to correct spectra of quinine sulfate solution in sulfuric acid and results corresponded well with standard spectra by Rance A. *et al.*[2]. Absorption spectra of both solutions (illuminated and kept in the

dark) were collected against recorded baseline (Cintra 404, GBC Scientific, 270 – 800 nm, step 0.2 nm, slit 2 nm) after 0, 10, 20, 30 and 40 min.

2.2. Data evaluation

Data were evaluated using MS Excel 2010 (Microsoft, USA). All measured spectra were corrected to absorption of PBS or DMEM+FBS. From concentrations and spectrum of photosensitizer absorbance of photosensitizer A_{PS} in solutions was estimated and then exposure $I_A(t)$ for solution illuminated for time t was calculated as

$$I_A(t) = \int_0^t \int_{\lambda_1}^{\lambda_2} \frac{I}{I_0}(\lambda) \cdot \left(1 - 10^{-A(\lambda,t)}\right) \cdot d\lambda dt$$

where $I/I_0(\lambda)$ is source relative emission intensity in photons per wavelength λ and $A(\lambda,t)$ is absorbance of photosensitizer at wavelength λ and time τ from the beginning of illumination. Wavelength integration limits were λ_1 = 450 nm and λ_2 = 750 nm and trapezoidal rule for integration was used for absorbance in intervals between spectral measurements. Eventually, chemical photodynamical efficiency γ_x of a photosensitizer was evaluated from single exponential dependence of relative uric acid concentration on light exposure

$$c_{rel,UA}(I_A(t)) = \exp[-\gamma_x I_A(t)]$$

Then quantum yields of photosensitizers were calculated using RB in PBS and DMEM+FBS, respectively, as a standard (ϕ[RB,PBS] = 0.75, according to ref. [3, 4]) using equation

$$\phi_x = \phi_{std} \gamma_x / \gamma_{std}$$

where ϕ_x is estimated quantum yield, ϕ_{std} is quantum yield of the standard and γ_x and γ_{std}, respectively, are chemical photodynamical efficiencies of an evaluated compound and a standard, respectively.

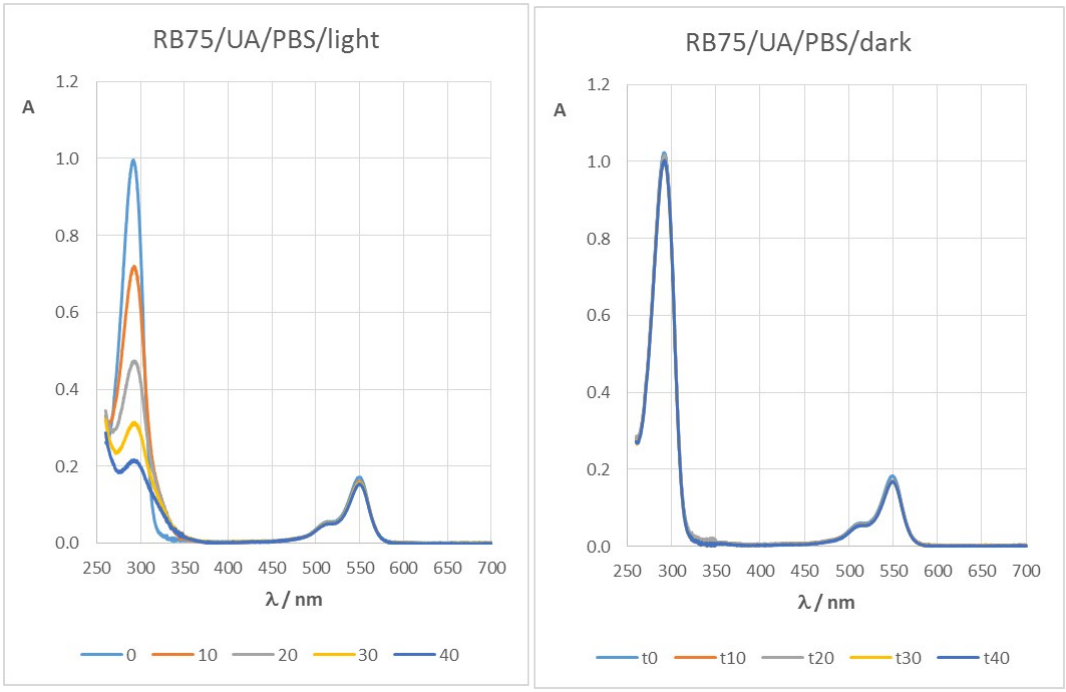

Fig. S10: Absorption spectra of Rose Bengal (RB) and uric acid mixture in phosphate buffered saline (PBS) measured at different times (0, 10, 20, 30, 40 min) after light exposure (left panel) or kept in dark (right panel)

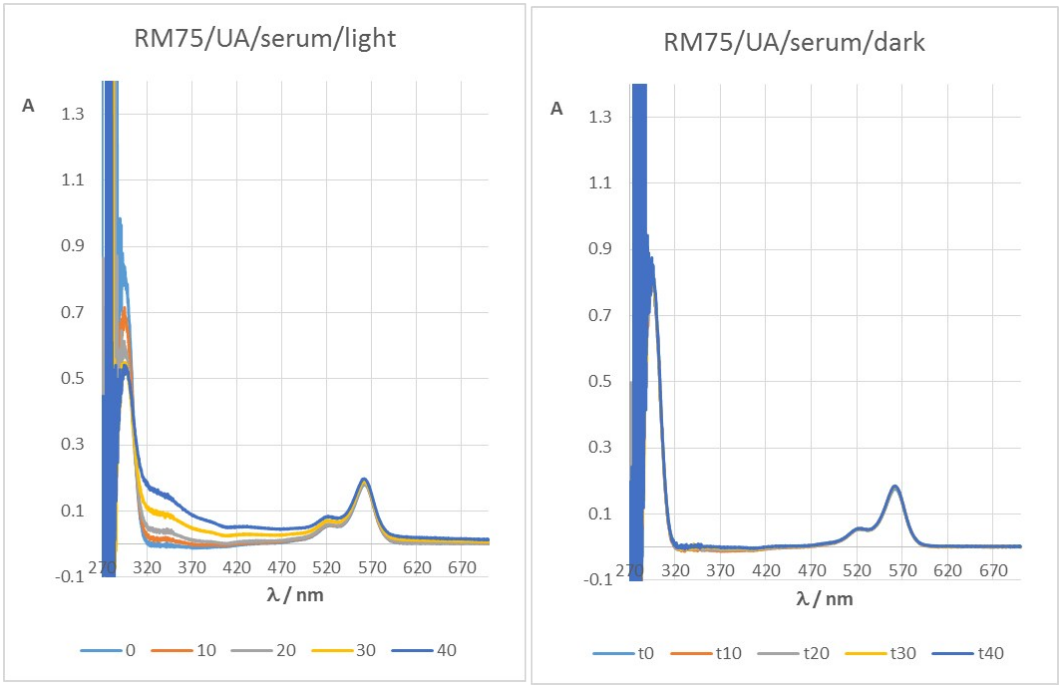

Fig. S11: Absorption spectra of Rose Bengal (RB) and uric acid mixture in Dulbecco's Modified Eagle Medium (DMEM) with fetal bovine serum measured at different times (0, 10, 20, 30, 40 min) after light exposure (left panel) or kept in dark (right panel)

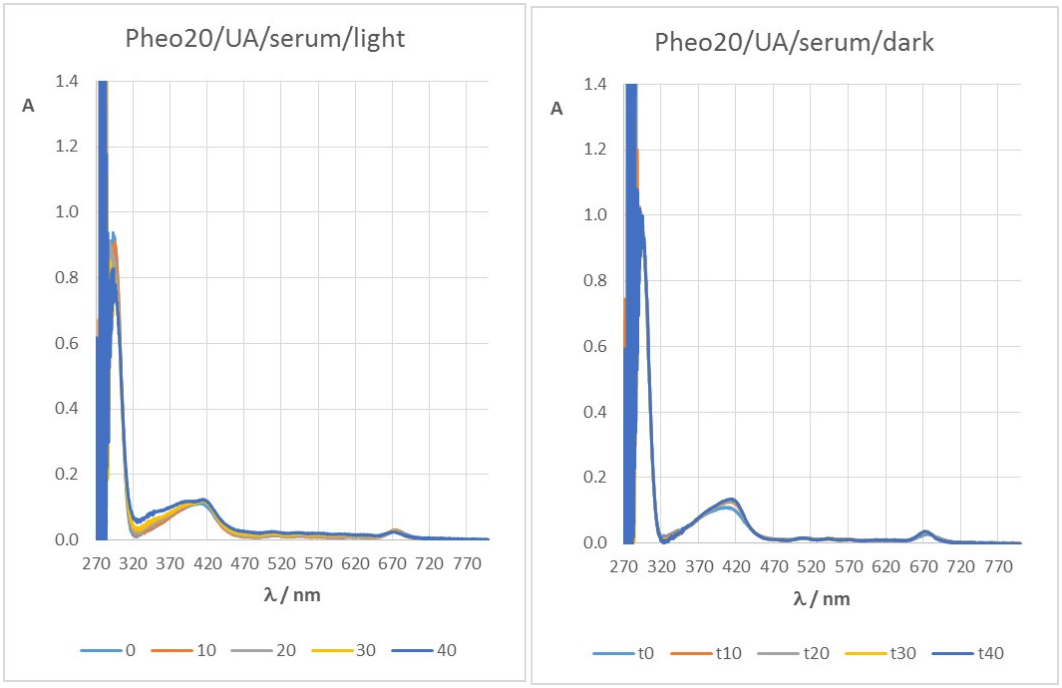

Fig. S12: Absorption spectra of Pb*a* and uric acid mixture in Dulbecco's Modified Eagle Medium (DMEM) with fetal bovine serum measured at different times (0, 10, 20, 30, 40 min) after light exposure (left panel) or kept in dark (right panel)

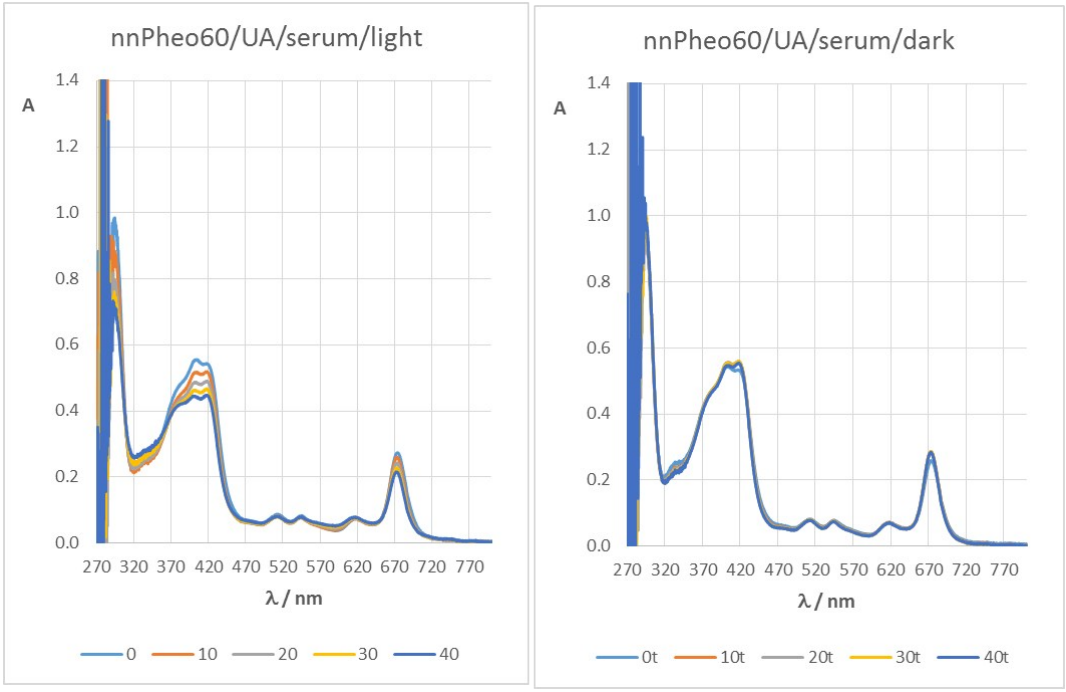

Fig. S13: Absorption spectra of NT-Pb*a* conjugate and uric acid mixture in Dulbecco's Modified Eagle Medium (DMEM) with fetal bovine serum measured at different times (0, 10, 20, 30, 40 min) after light exposure (left panel) or kept in dark (right panel)

3. *In vitro* cell studies

3.1 Cell lines and culture conditions

In this study we used the following human cell lines: LNCaP (prostate carcinoma, $PSMA^+$), PC-3 (prostate carcinoma), MCF-7 (breast carcinoma), U-2 OS (cells from osteosarcoma), AR U-2 OS (cells from osteosarcoma stably expressing the androgen receptor) and HEK 293T (embryonic kidney cells); and one mouse cell line C2C12 (myoblasts). Cell lines were purchased from American Type Culture Collection (ATCC, Manassas, VA), except AR U-2 OS which was kindly provided by Dr. David Sedlak from the CZ-OPENSCREEN: National Infrastructure for Chemical Biology, Institute of Molecular Genetics AS CR.

Unless otherwise specified the cells were cultured in medium (Sigma-Aldrich, USA) recommended by ATCC, supplemented with 10% FBS (Thermo-Fisher, USA) and 2 mM L-Glutamine (Sigma-Aldrich, USA). Cells were maintained at exponential growth phase under standard physiological conditions at 37 °C in humidified atmosphere with 5% CO_2.

3.2 Evaluation of photo- and dark toxicity of pheophorbide *a* and its nandrolone conjugate

Photo- and dark toxicity of the tested compounds was determined by WST-1 assay (Sigma, USA), similar as in Jurášek *et al.* (2014)[5], which is based on reduction of tetrazolium salt (WST-1 substrate) into soluble formazan by activity of mitochondrial oxidoreductases in metabolically active cells. The arisen formazan was measured spectrophotometrically at 450 nm (reference wavelength 655 nm) using UV–Vis spectrometer (Tecan). The measured absorbance is directly proportional to the amount of arisen formazan, which is proportional to the oxidoreductase activity, and therefore, to the number of metabolically active cells.

For this assay, LNCaP, PC-3, MCF-7, U-2 OS, AR U-2 OS, C2C12 and HEK 293T cells were seeded into individual wells of 96-well plates (7,500 cells per well) in 100 μL of cell culture medium (MCF-7, U-2 OS, AR U-2 OS and HEK 293T in DMEM medium, PC-3 in Ham´s medium) supplemented with 10% FBS. The cells were incubated overnight (14 h) under standard cultivation conditions (37 °C, 5% CO_2, 95% humidity). LNCaP were inoculated in Iscove's medium (10,000 cells per well) and incubated for 24 h due to their longer generation time. After the incubation period, 100 μL of fresh media with the tested compounds (final concentration 0-20 μM) was added. The cells were cultivated in the absence of light for another 24, 48 and 72 h under standard conditions. Next, the medium was removed and the cells were incubated with 5 μL of WST-1 dissolved in 100 μL of complete medium without phenol red for 2 h. The absorbance was measured. Cells incubated with medium without any compound were used as control. All experiments were done in quadruplicates. The data were analyzed by

GraphPad Prism 6.0 and the IC_{50} values (half inhibitory concentrations) were determined using non-linear regression (function dose response). The deviations were calculated as standard error of the mean (SEM).

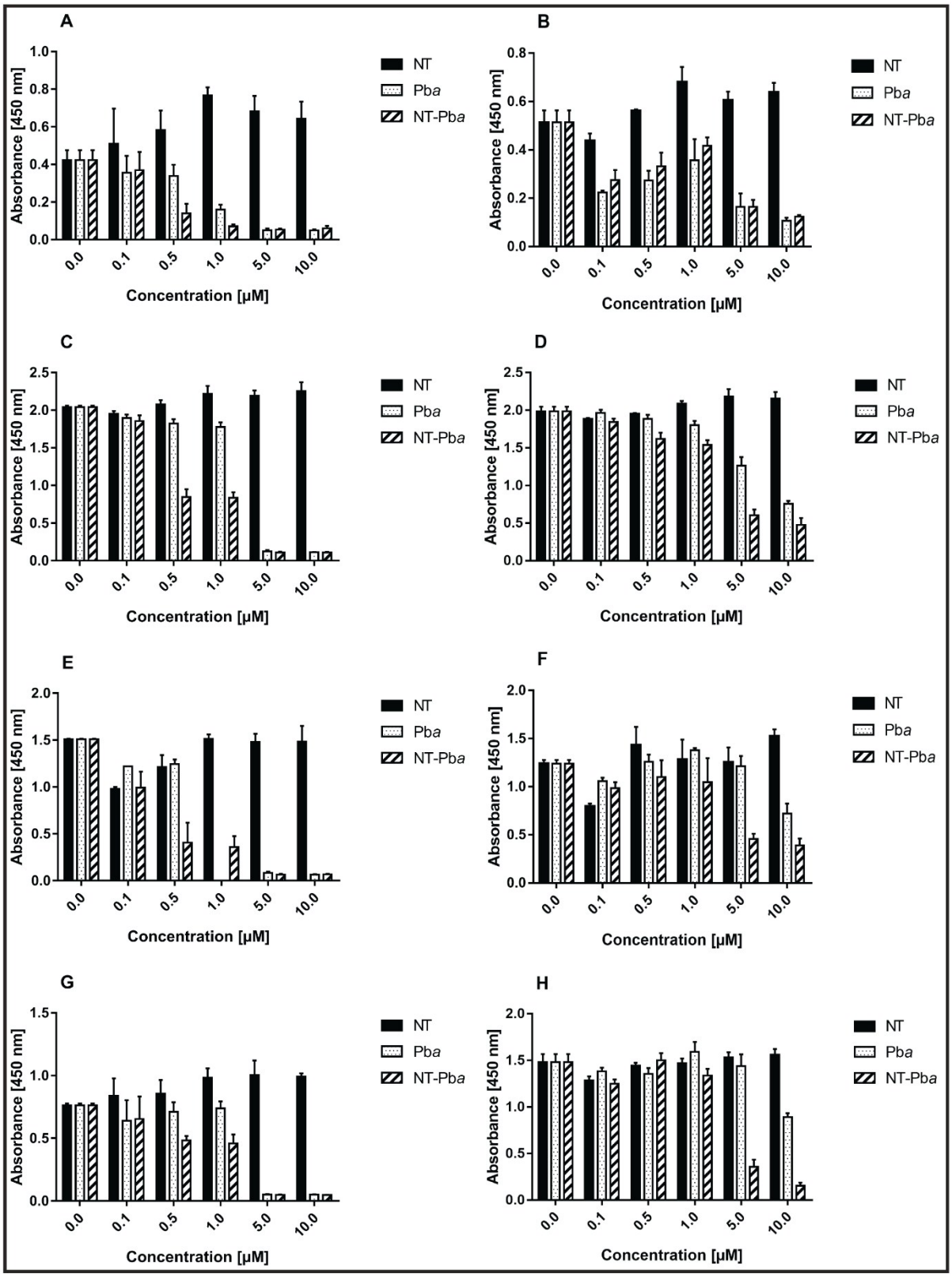

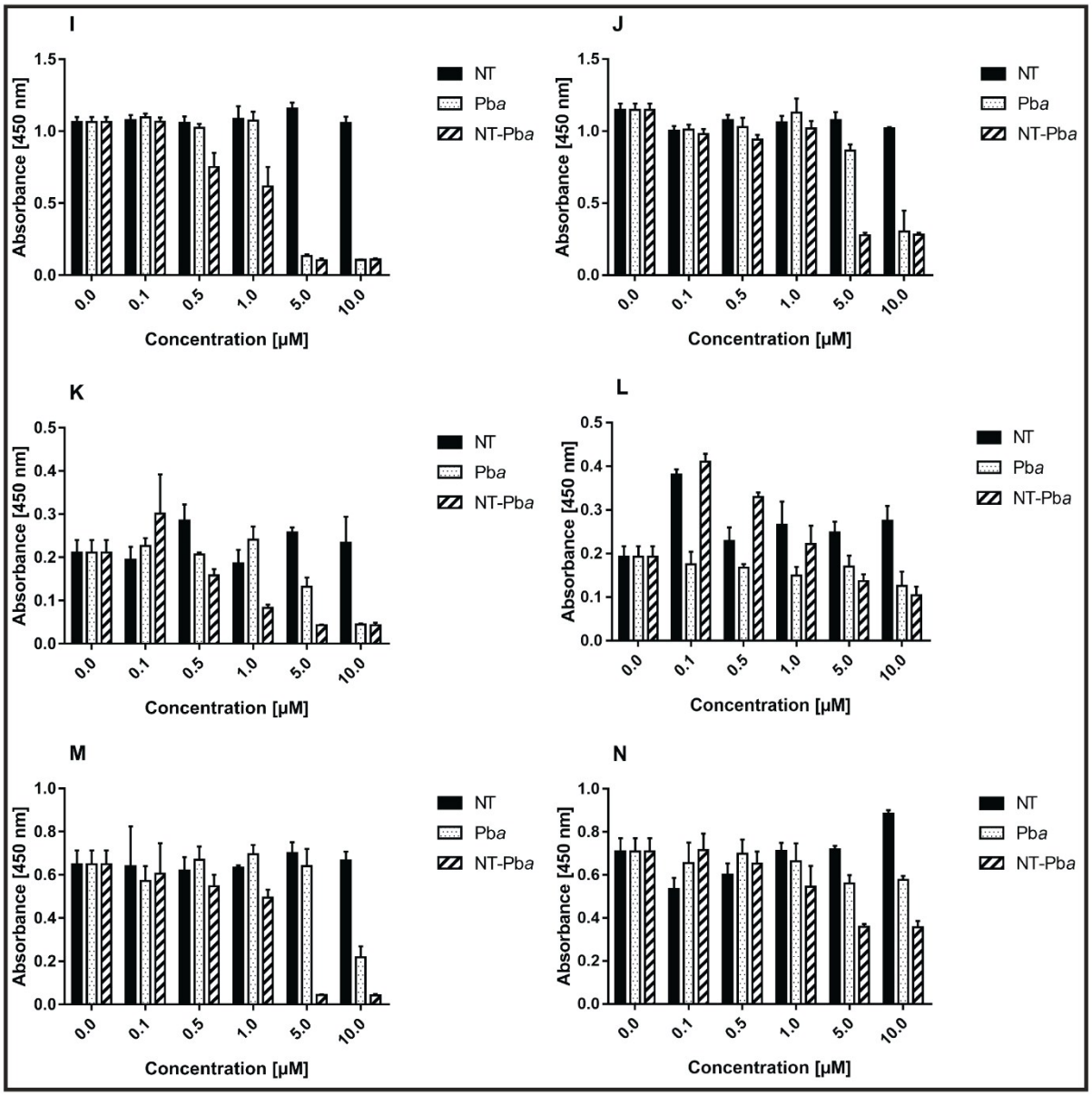

Fig. S18: Photo- and dark toxicity of NT-Pb*a in vitro*. Cell viability determined by WST-1 assay after 24 h of incubation with the tested compounds. A, B) LNCaP; C, D) PC-3; E, F) AR U-2 OS; G, H) U-2 OS; I, J) MCF-7; K, L) HEK-293T and M, N) C2C12 cells. A, C, E, G, I, K, M) Phototoxicity (cell viability after compound photoactivation) and B, D, F, H, J, L, N) dark toxicity (cells kept in the dark after NT-Pb*a* treatment).

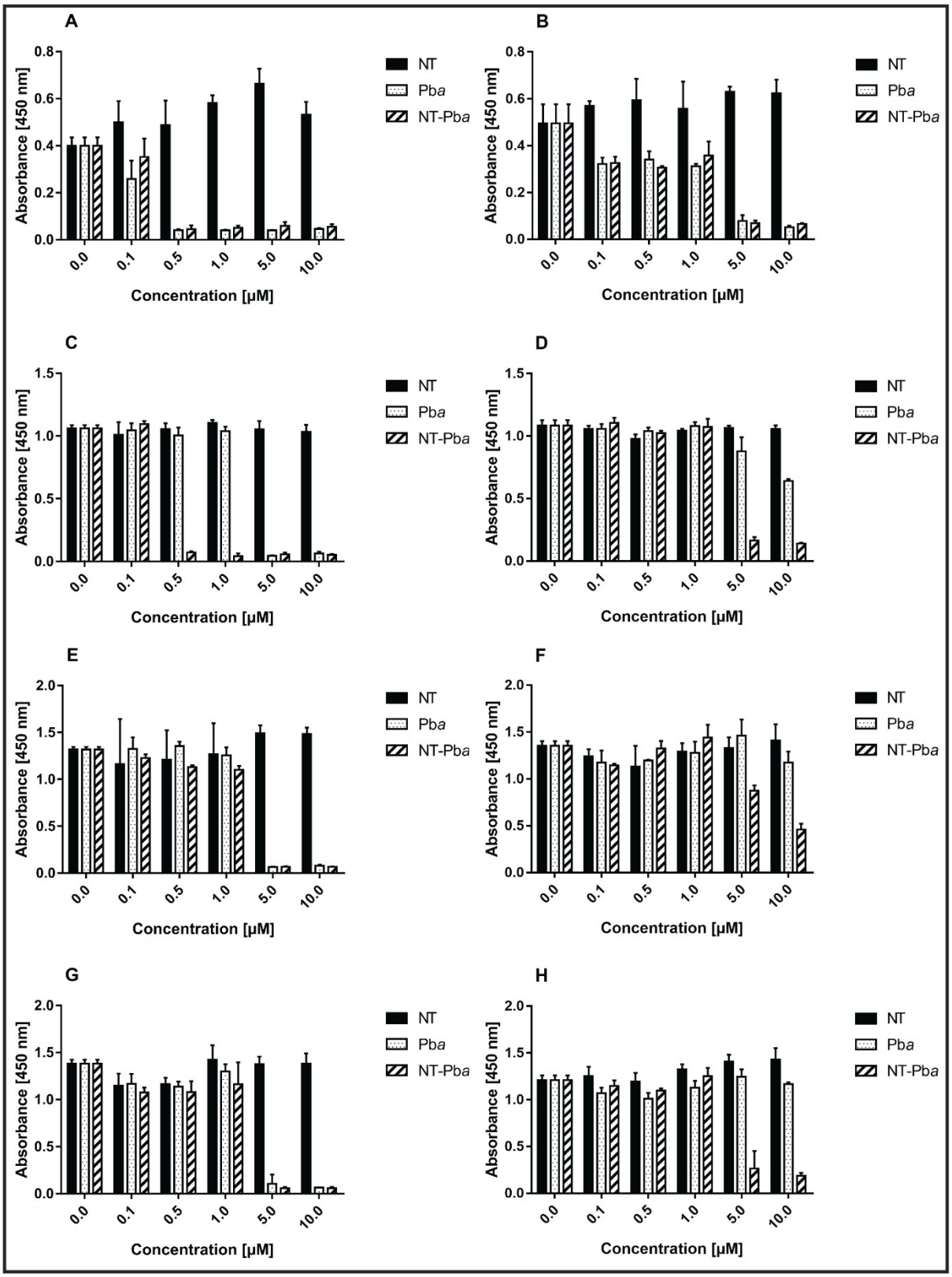
A
B
C
D
E
F
G
H
Absorbance [450 nm]
Concentration [μM]
0.0
0.1
0.5
1.0
5.0
10.0
NT
Pba
NT-Pba

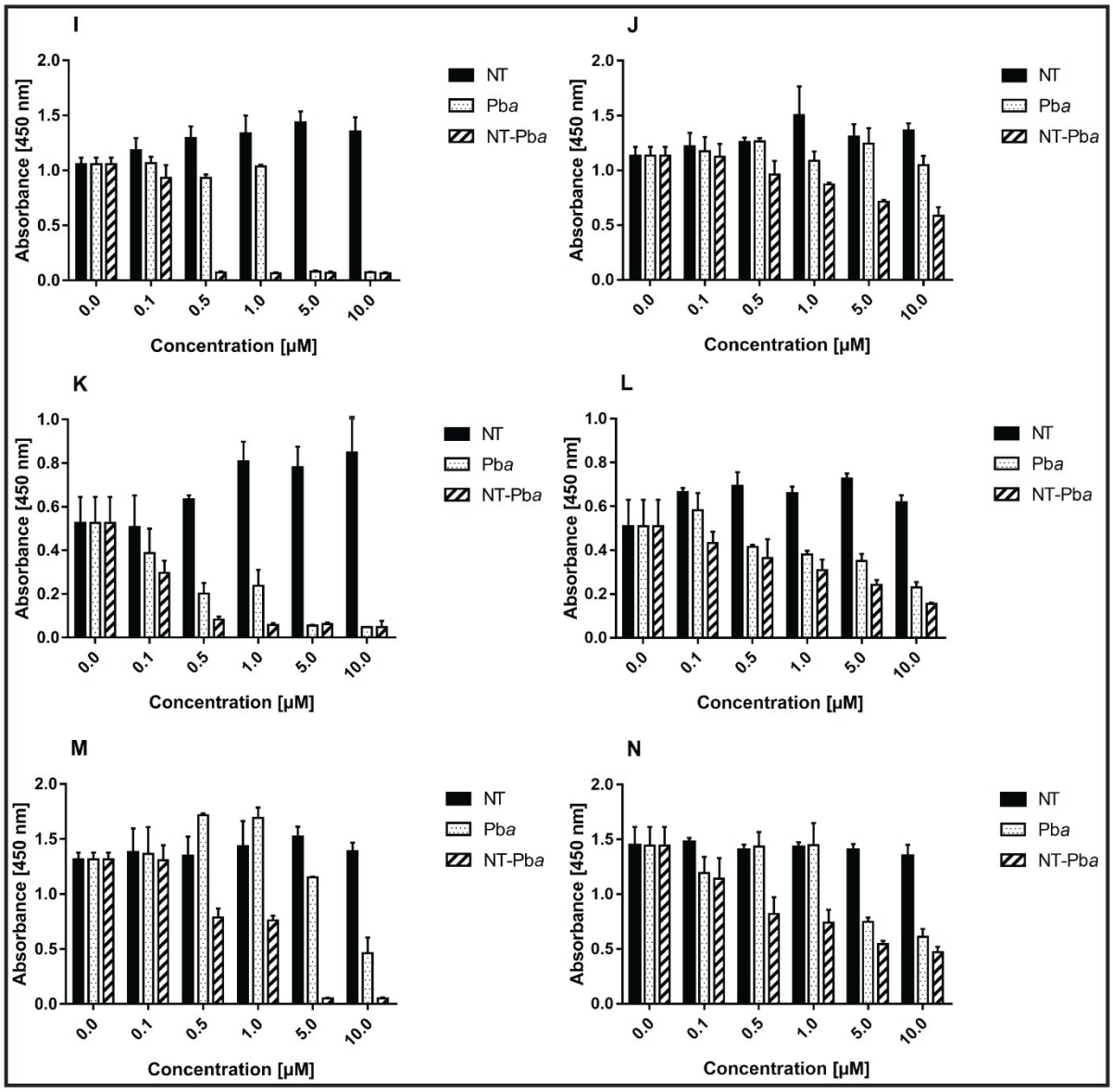

Fig. S19: Photo- and dark toxicity of NT-Pb*a in vitro*. Cell viability determined by WST-1 assay after 48 h of incubation with the tested compounds. A, B) LNCaP; C, D) PC-3; E, F) AR U-2 OS; G, H) U-2 OS; I, J) MCF-7; K, L) HEK-293T and M, N) C2C12 cells. A, C, E, G, I, K, M) Phototoxicity (cell viability after compound photoactivation) and B, D, F, H, J, L, N) dark toxicity (cells kept in the dark after NT-Pb*a* treatment).

Table S1: Photo- and dark toxicity of NT-Pb*a*, Pb*a* and NT in human cancer cell lines *in vitro* after 48 h of incubation.

IC_{50}[a] [μM]

Compound	**NT**		**Pb*a***		**NT-Pb*a***	
Cell line	Illumination	Dark	Illumination	Dark	Illumination	Dark
AR U-2 OS	> 10	> 10	2.14 ± 0.21	> 10	1.70 ± 0.04	3.72 ± 0.03
U-2 OS	> 10	> 10	1.46 ± 0.04	> 10	1.48 ± 0.07	2.39 ± 0.05
LNCaP	10	> 10	0.10 ± 0.04	2.65 ± 0.01	0.17 ± 0.04	2.57 ± 0.01
HEK-293T	> 10	> 10	0.32 ± 0.02	0.83 ± 0.01	0.09 ± 0.03	0.76 ± 0.05
MCF-7	> 10	> 10	1.83 ± 0.010	> 10	0.14 ± 0.07	>10
C2C12	> 10	> 10	3.81 ± 0.00	2.52 ± 0.12	0.79 ± 0.02	0.28 ± 0.10
PC-3	> 10	> 10	1.97 ± 0.02	> 10	0.22 ± 0.01	2.11 ± 0.03

[a]IC_{50} - half maximal inhibitory concentration

Table S2: Phototoxicity of pheophorbide *a* and its conjugates in selected cell lines.

Compound	Target	IC_{50}[a] [nM]	Cell line	Light dose [J/cm^2]	λ [nm]	t [h]	Reference
DR2 (Pb*a*-Nonsteroidal anti-androgen)	Androgen receptor	2.53⓾10^1	VCaP	7.2	White-light	24	[6]
		1.2 ⓾10^1	LNCaP				
		3.51⓾10^1	PC-3				
Estradiol-Pb*a* (3)	Estrogen receptor	85	MCF-7	8.2	400	48	[7]
Estradiol-Pb*a* (4a)		83					
Estradiol-Pb*a* (4b)		13					
Clorin e6-guanidin (3)	Mitochondria	5.45⓾10^2	A549	2	650	4	[8]
Clorin e6-guanidin (4)		1.97⓾10^2		1.7	660		
Clorin e6-curcumin (17)	Not target specific	3.5⓾10^1	MIA PaCa-2	9	660	72	[9]
		4⓾10^1	AsPC-1				
		4.1⓾10^1	PANC-1				
Chlorine A		3.8⓾10^2	Eca-109 cells	2	650	4	[10]
Porphin (P1-4)		8.19-12.5⓾10^3	Eca-109 cells	16	635		[11]
Chlorin (C1-4)		2.65-3.31⓾10^3	Eca-109 cells	16	650	24	
Bacteriochlorin (B1-4)		2.43-3.09⓾10^3	Eca-109 cells	16	730		
Pb*a*		9.8⓾10^2	PC-3	2	630	24	[12]
		7⓾10^1	MCF-7	14	n.a.		[30]
		1.5⓾10^2	HeLa				
		9.5⓾10^1	HepG2				
		2.5⓾10^2	B78-H1				
		5⓾10^2	MCF-7	84	610	2	[31]
		n.a.[b]	LNCaP	5	670	24	[32]
		1.5⓾10^3	HepB3	84	610	48	[33]

[a] phototoxic (after illumination) half maximal inhibitory concentration

[b] n.a. – information not available in the manuscript

3.3 Intracellular localization

The intracellular localization of NT-Pb*a* was studied by real-time live-cell fluorescence microscopy (37 °C, 5% CO_2 atmosphere). The images were acquired by an inverse fluorescence microscope (Olympus IX-81, xCellence software), high-stability 150 W xenon arc burner, EM-CCD camera C9100-02 (Hamamatsu, Germany). Living cells were analyzed by a 60× oil immersion objective (Olympus, Japan) with the numerical aperture of 1.4 using a set of Olympus filters: U-MWU-2, U-MNB2, U-MNG2, U-MWIY2 and U-DM-CY5. All images were deconvolved by xCellence basic deconvolution module.

3.4 Cell uptake study

The intracellular localization of NT-Pb*a* was studied by real-time live-cell fluorescence microscopy (set-up as described in Section 3.3. Cells ($1 \cdot 10^5 \cdot well^{-1}$) were seeded on 35 mm glass bottom dishes for live-cell imaging (MatTek Corporation, USA) and left to adhere 14 h (except of LNCaP, 24 h). The attached cells were washed with PBS (pH 7.4, 37 °C) and incubated with nandrolone derivatives (0.2 – 1 μM) dissolved in complete cell culture phenol red-free medium at 37 °C for 0.5 - 24 h. Stock solutions of the tested compounds were prepared fresh before each experiment in DMSO. The final DMSO concentration in culture medium did not exceed 0.05%. After the incubation period, the cells were washed twice with PBS and fresh phenol red-free medium was added.

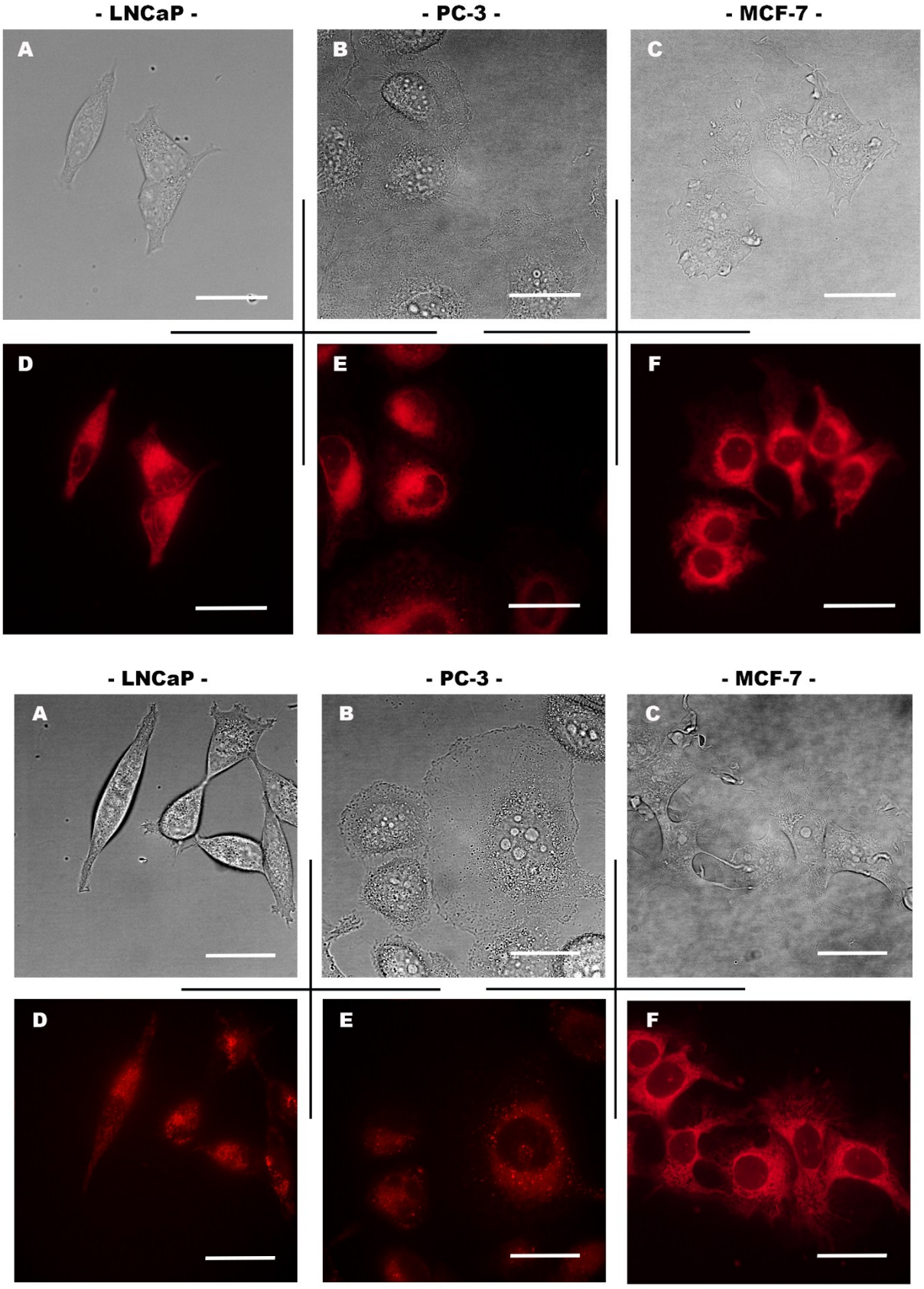

Fig. S20: Fluorescence microscopy images of intracellular localization of NT-Pb*a* in human cancer cells *in vitro*. NT-Pb*a* was applied in 1 µM concentration for 3 (upper panel) and 20 h (lower panel) in human cancer cells derived from prostate LNCaP (A, D) and PC-3 (B, E), and from breast MCF-7 (C, F). The scale bar represents 20 µm.

3.5 Determination of cell organelle localization

Cells were seeded in glass bottom dishes (MatTek Corporation, USA) and left overnight to adhere. Then, they were rinsed with PBS and exposed to the tested compounds dissolved in complete medium. To assess their exact intracellular localization, we used endoplasmic reticulum marker ER-Tracker™ Blue-White (30 min, 100 nM; ThermoFisher Scientific, USA), mitochondrial marker MitoTracker™ Green (15 min, 70 nM; Invitrogen, USA) and lysosomal marker LysoTracker™ Green (15 min, 70 nM; Invitrogen, USA).

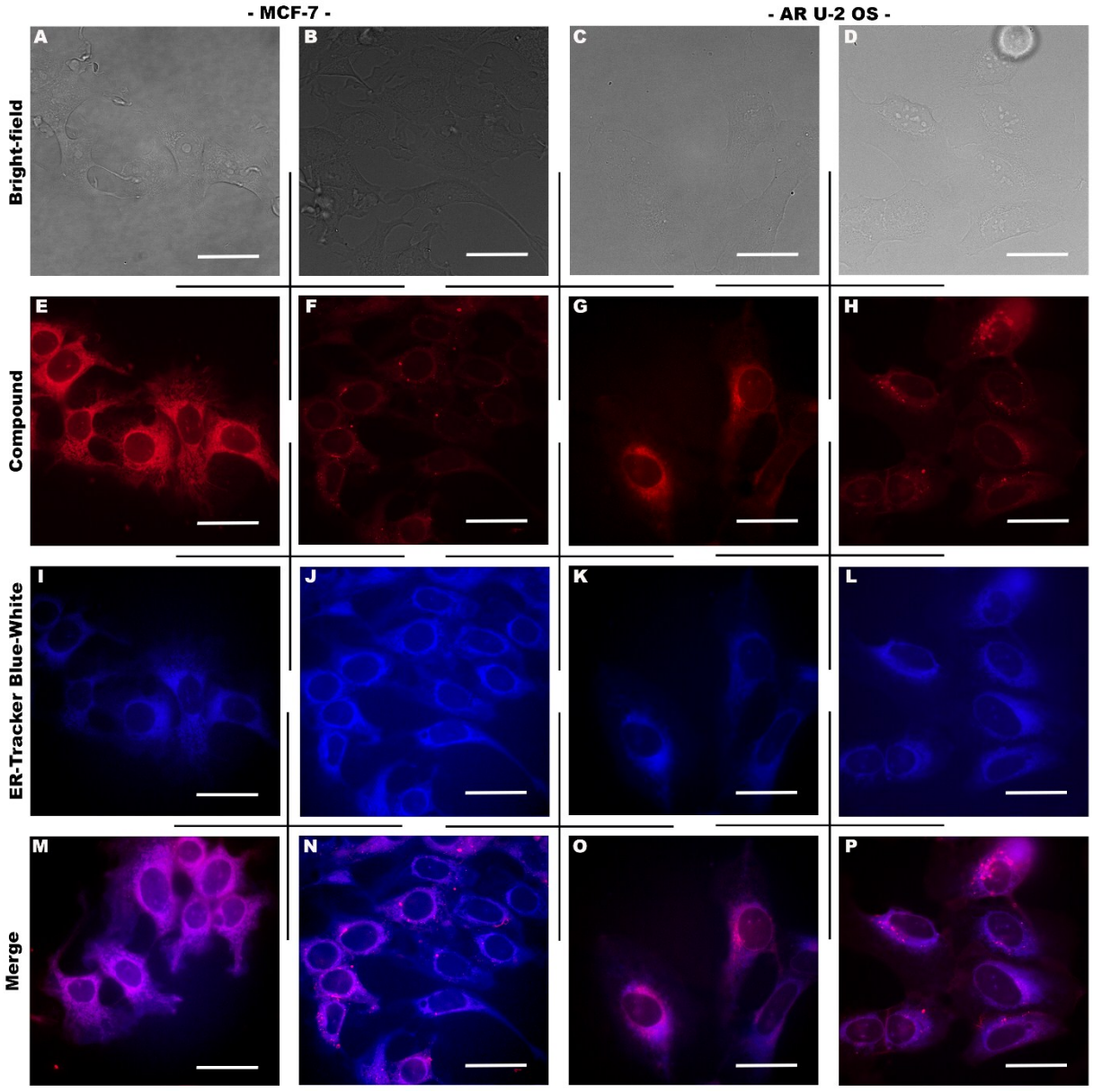

Fig. S21: Fluorescence microscopy images of NT-Pb*a* and Pb*a* localization in endoplasmic reticulum of human cancer cell lines. Colocalization of NT-Pb*a* or Pb*a* (100 nM, 3 h) with ER-Tracker™ Blue-White DPX (70 nM, 30 min.) in MCF-7 and AR U-2 OS cells: A-D) Bright-field images; E, G) NT-Pb*a* conjugate localization; F, H) Pb*a* localization, I-L) ER-Tracker™ Blue-White DPX, M-P) merge. The scale bar represents 20 μm.

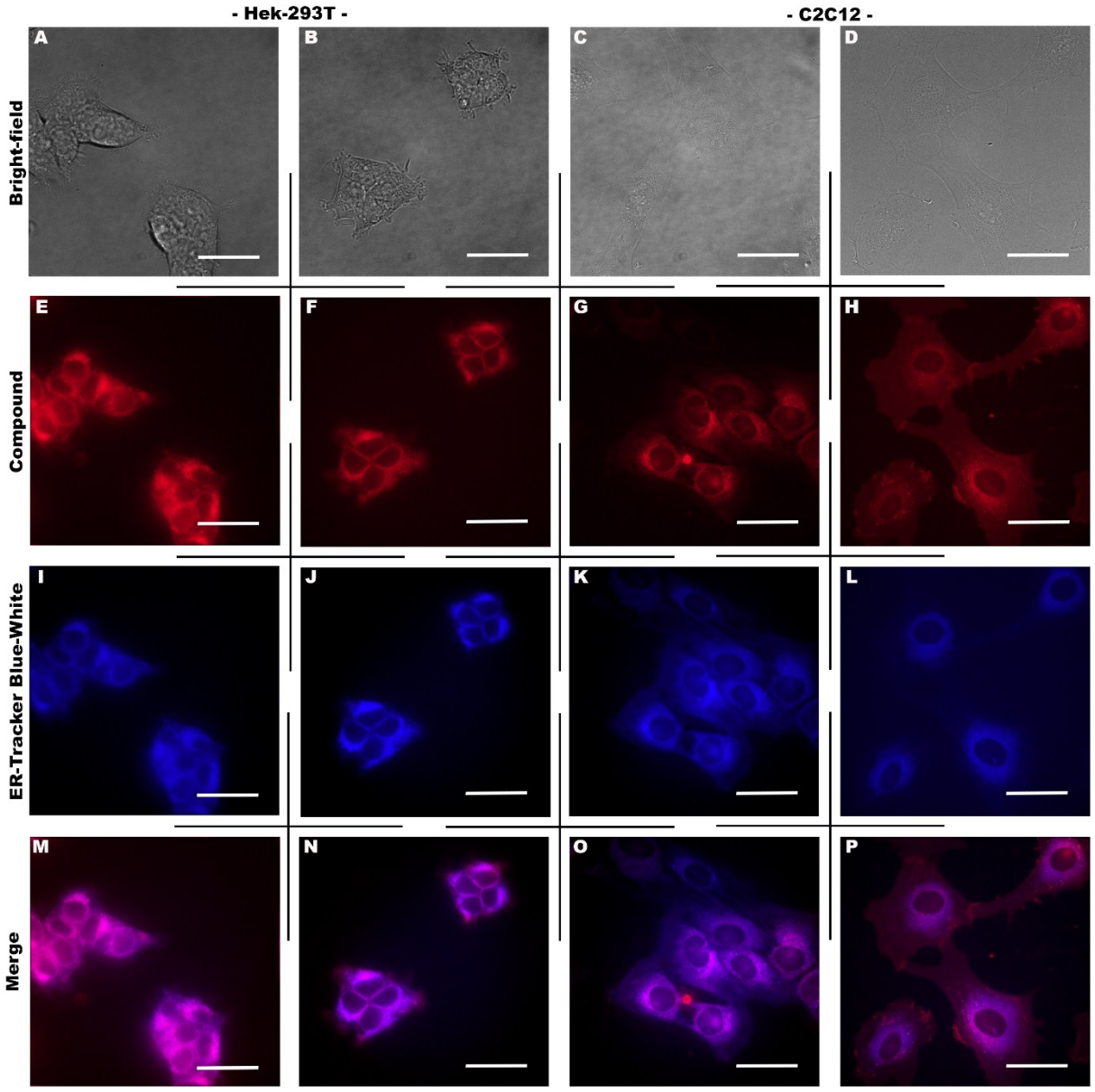

Fig. S22: Fluorescence microscopy images of NT-Pb*a* and Pb*a* localization in endoplasmic reticulum of human cancer cell lines. Colocalization of NT-Pb*a* or Pb*a* (100 nM, 3 h) with ER-Tracker™ Blue-White DPX (70 nM, 30 min.) in HEK 293T and C2C12 cells: A-D) Bright-field images; E, G) NT-Pb*a* conjugate localization; F, H) Pb*a* localization, I-L) ER-Tracker™ Blue-White DPX, M-P) merge. The scale bar represents 20 μm.

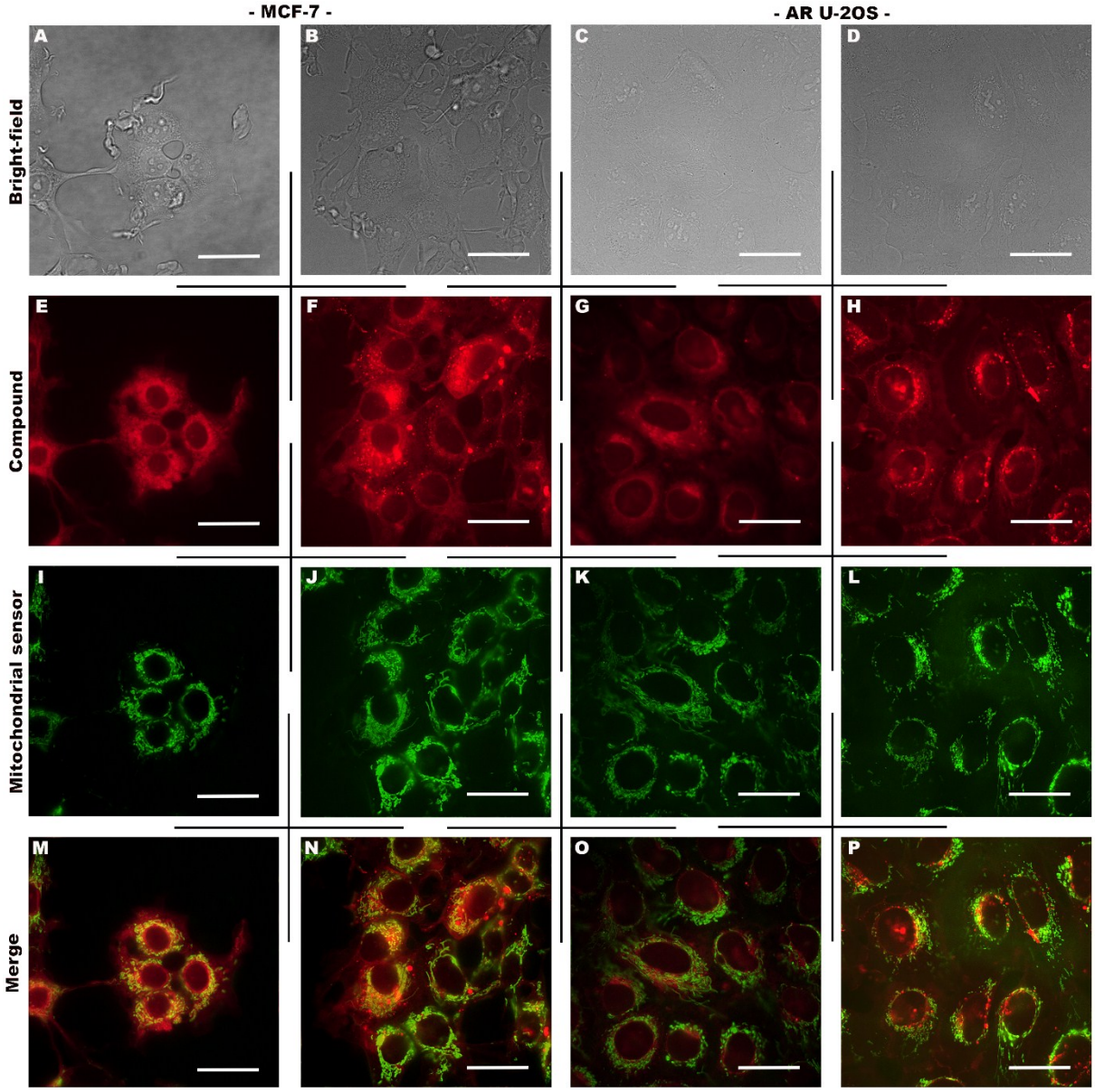

Fig. S23: Fluorescence microscopy images of NT-Pb*a* and Pb*a* localization in mitochondria of human cancer cell lines. Colocalization of NT-Pb*a* or Pb*a* (100 nM, 3 h) with MitoTracker™ Green FM (15 min, 70 nM) in MCF-7 and AR U-2 OS cells: A-D) Bright-field images; E, G) NT-Pb*a* conjugate localization; F, H) Pb*a* localization, I-L) MitoTracker™ Green FM, M-P) merge. The scale bar represents 20 μm.

*For AR U-2 OS, a green-emitting mitochondria-specific dye based on a dimethinium salt from Bříza *et al.* (2017)[13] was used, since MitoTracker Green FM strongly binds extracellular matrix[14] and enhances fluorescent background.

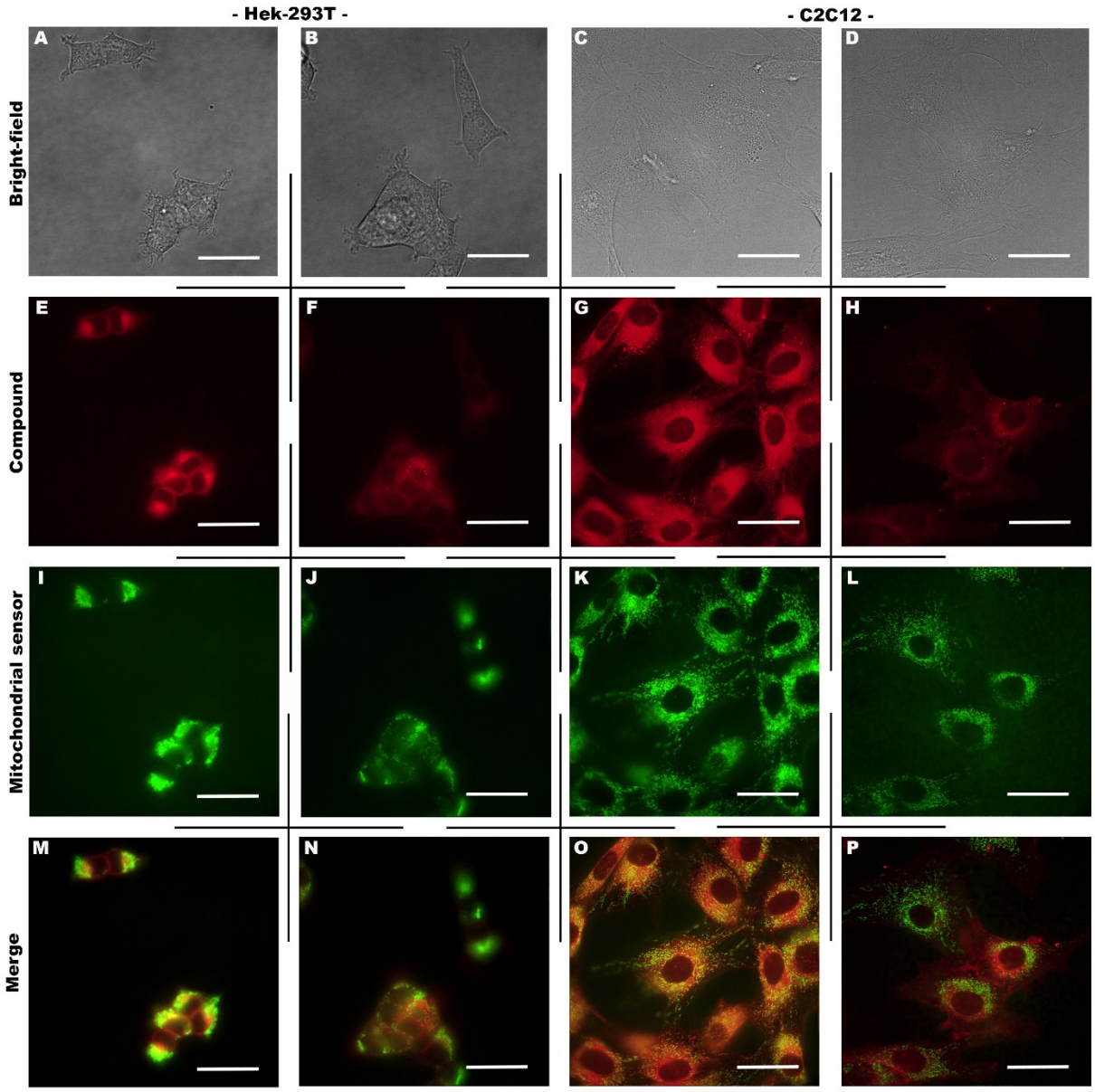

Fig. S24: Fluorescence microscopy images of NT-Pb*a* and Pb*a* localization in mitochondria of human cancer cell lines. Colocalization of NT-Pb*a* or Pb*a* (100 nM, 3 h) with MitoTracker™ Green FM (15 min, 70 nM) in HEK 293T and C2C12* cells: A-D) Bright-field images; E, G) NT-Pb*a* conjugate localization; F, H) Pb*a* localization, I-L) MitoTracker™ Green FM, M-P) merge. The scale bar represents 20 μm.

*For C2C12, a green-emitting mitochondria-specific dye based on a dimethinium salt from Bříza *et al.* (2017)[13] was used, since MitoTracker Green FM strongly binds extracellular matrix[14] and enhances fluorescent background.

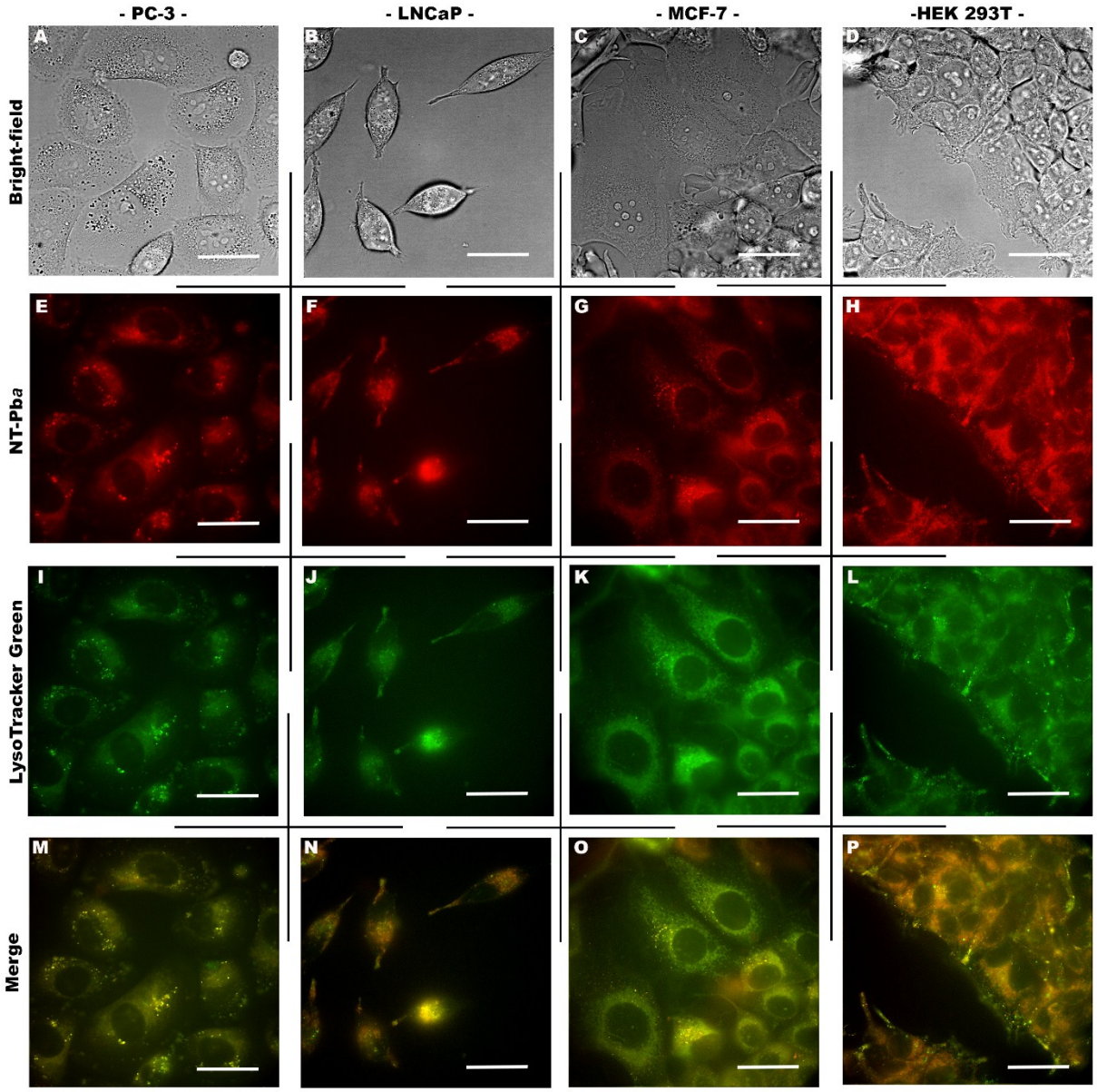

Fig. S25: Fluorescence microscopy images of NT-Pb*a* and Pb*a* localization in lysosomes of human cancer cell lines. Colocalization of NT-Pb*a* or Pb*a* (100 nM, 3 h) with LysoTracker™ Green FM (15 min, 70 nM) in PC-3, LNCaP, MCF-7 and HEK 293T cells: A-D) Bright-field images; E, G) NT-Pb*a* conjugate localization; F, H) Pb*a* localization, I-L) LysoTracker™ Green FM, M-P) merge. The scale bar represents 20 μm.

3.6 Fluorescence competitive assay

MCF-7 cells ($1 \cdot 10^5 \cdot well^{-1}$) were seeded on microscopic dishes with grid (μ-Dish 35mm Grid-500; Ibidi, Germany) in medium with charcoaled FBS (steroid and other small compounds depletion) and left to adhere for 24 h. Then, the cells were washed by PBS and influenced with NT-Pb*a* or Pb*a* derivatives at 0.2 μM concentration for 3 h. After the incubation period, the cells were washed by PBS and the fluorescence emission of the intracellularly localized NT-Pb*a* or Pb*a* was recorded in living cells in a number of view fields. Then, fresh phenol-

red free medium supplemented with charcoaled FBS with the addition of 50-fold excess of competitive androgens NT and testosterone was added to the cells for another 1.5 h, after which the cells were imaged at the same exposure time and light intensity.

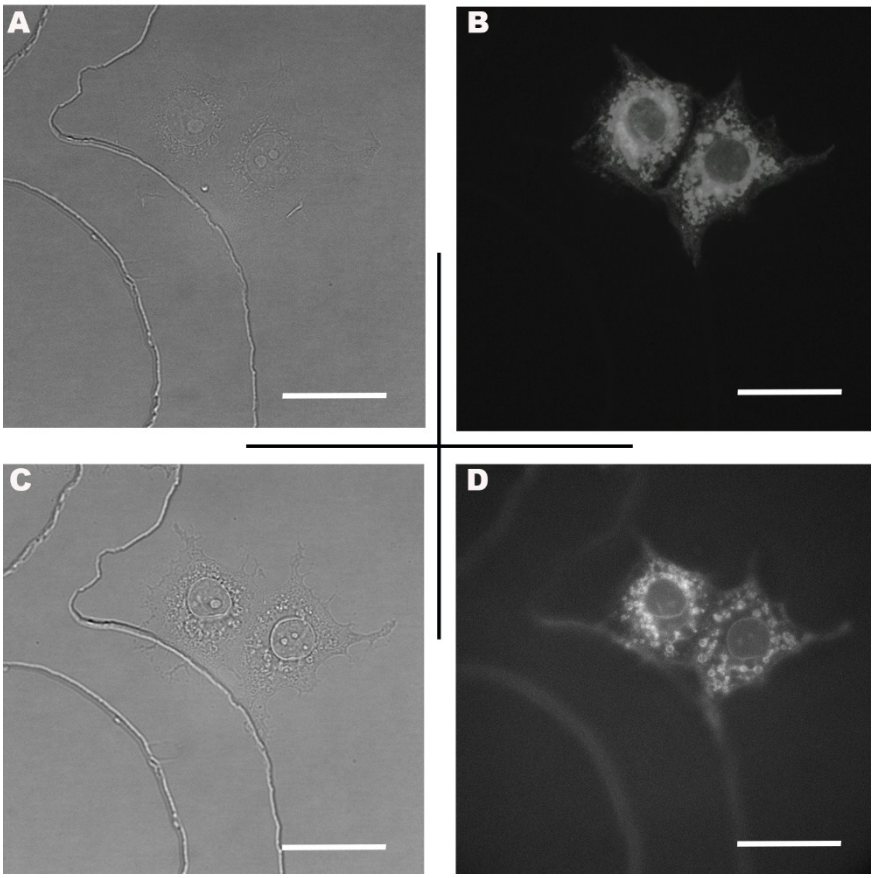

Fig. S26. NT-Pb*a* cellular uptake in a competitive assay with nonfluorescent testosterone. A) Bright-field image of MCF-7 cells; B) fluorescent image of intracellular localization of NT-Pb*a* (3 h, 0.2 μM); C) Bright-field image of MCF-7 cell after additional 1.5 h; D) Displacement of NT-Pb*a* with 50-fold excess of nonfluorescent testosterone after 1.5 h of competition with localized NT-Pb*a*. The same MCF-7 cells were found in bright field using Ibidi microscopic dishes with a grid (μ-Dish 35mm Grid-500). The scale bars represent 20 μm.

3.7 Steroid receptor reporter luciferase assays

Transcriptional response of steroid receptors to tested compounds was evaluated using a panel of U-2 OS reporter cell lines stably expressing human full-length steroid receptors as previously described[15]. In the ERα reporter cell line, luciferase expression is driven by 3 repeats of estrogen response elements (ERE) while viral promoter derived from MMTV LTR controls the expression of luciferase in the AR reporter cell line. At the time of 24 h before the experiment, the growth medium was changed for phenol red-free DMEM supplemented with

4% HyClone FBS, charcoal/dextran treated, (GE Healthcare Life Sciences, USA) and 2 mM Glutamax (starvation medium). The cells were harvested, counted and seeded into cell culture-treated, white, solid 1536-well plates (Corning Inc.) at 1,500 cells per well in 5 µL of total media volume. The tested compounds were diluted in DMSO and were transferred to cells using contact-free acoustic transfer by ECHO 520 (Labcyte, Inc.). The cells were incubated with the tested compounds for 24 h, then, the luciferase activity was measured with Britelite plus luciferase reporter gene assay reagent (Perkin Elmer) by a multimode plate reader Envision (Perkin Elmer). The data were analyzed using an in-house developed Laboratory Information Management System (LIMS).

3.8 Translocation of androgen receptor

The number of $1 \cdot 10^5$ U-2 OS cells was seeded into glass bottom dishes and cultured in phenol red-free DMEM supplemented with 2% charcoal-treated FBS. Then, 2 h after seeding, the cells were transfected with 500 $ng \cdot \mu L^{-1}$ of pEGFP-C1-AR plasmid DNA (Addgene, USA; number 28235) using Fugene® HD (Promega, USA) according to the manufacturer´s instructions. Then, 24 h after the transfection, the cells were treated with NT-Pb*a* at 10, 100, 200 and 500 nM concentrations and incubated for further 1 and 24 h. Pure NT (the same concentrations) and Pb*a* served as positive and negative control, respectively. Then, translocation of the androgen receptor into the cell nucleus was monitored by live-cell fluorescence microscopy.

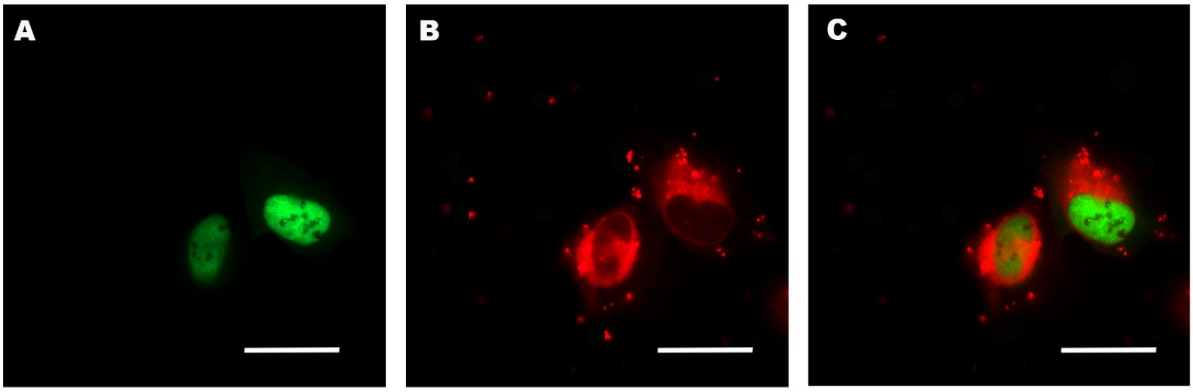

Fig. S27. Nuclear translocation of the androgen receptor (AR) in human cells from osteosarcoma after NT-Pb*a* treatment. Fluorescence microscopy images of U-2 OS cells transiently transfected with pEGFP-C1-AR plasmid DNA for 20 h. A) AR-GFP translocation induced by NT-Pb*a*, B) NT-Ph*a* (500 nM, 1 h), C) merge of images A and B. The scale bars represent 20 µm

4. Evaluation of intracellular cleavage of NT-Pb*a*

4.1 Cell fractionation

U-2 OS cells were seeded into 10-cm dish in DMEM supplemented with 10% FBS. Then, 2.5 h after seeding, the cells were transfected with 0.5 $\mu g.\mu L^{-1}$ pEGFP-C1-AR plasmid DNA (Addgene, USA) in OptiMEM (Sigma, USA) using Fugene® HD (1:3 ratio, Promega, USA) according to the manufacturer´s instructions. After 24 h, the medium was changed and the cells were treated with 500 nM NT-Pb*a* for 24 h. Nuclear and cytosolic fraction was prepared as it is described in the protocol. Briefly, the cells were washed by PBS, detached from the cell cultivation dish by a scraper and transferred into an Eppendorf tube. Then, the tubes with cell suspension were centrifuged at 600 × g, for 10 min. (4 °C) and the supernatant was discarded. The cell pellet was resuspended in 0.1% NP-40 (Sigma-Aldrich, USA) solution in PBS, which was followed by centrifugation at 7,000 × g for 10 min. (4 °C); cytosolic and nuclear fractions were obtained. The nuclear fraction was dissolved in ice-cold PBS and the samples were immediately used for HRMS-ESI measurement.

4.2 NT-Pb*a* degradation determination by LC-MS/MS

The presence of NT in cell lysates was determined using LC-MS/MS method with derivatization reaction with 2-hydrazinopyridine. Briefly, 500 µL of cell lysate (in PBS) was diluted with 500 µL of the physiological solution. Samples were extracted with 3 mL of Et_2O. While the water phase was frozen in solid carbon dioxide, the organic phase was transferred into a glass tube and ether was evaporated. The samples were further derivatized by 100 µL of freshly prepared 2-hydrazinopyridine solution (1 mg of 2-hydrazinopyridine: 5 mL MeOH : 1.63 µL TFA). The samples were vortexed and then sonicated for 15 min at 50 °C, followed by evaporation of the solvents. Dry residues were reconstituted in 100 µL of 10 mM ammonium formate in 60% MeOH. The amount of 50 µL of the solution was injected into the LC-MS/MS.

4.3 LC-MS/MS analysis

LC-MS/MS was conducted by an API 3200 triple stage quadrupole mass spectrometer (Sciex, Concord, Canada) with electrospray ionization (ESI) connected to an ultra-high performance liquid chromatograph (UHPLC) Eksigent ultraLC 110 system (Redwood City, CA, USA) equipped with a refrigerated autosampler (4 °C) and a column heater (50 °C). The Kinetex C18 2.6 µm (150×3.0 mm) column (Phenomenex, Torrance, CA, USA) with a corresponding security guard was chosen for chromatographic separation at the flow rate of 0.75 $mL \cdot min^{-1}$ at 50 °C. The mobile phase consisted of water (solvent A) and methanol (solvent B). The following

gradient was employed (all steps were linear): 0 min, 40:60 (A:B); 2 min, 40:60; 6 min, 2:98; 8 min, 0:100; 8 min 20 s, 0:100, 8 min 23 s, 40:60; 11 min, 40:60 and at 11 min stop. The retention time of the analyte was 6.01 min.

Mass spectrometer detection was in the positive ESI mode using multiple-reaction monitoring transitions (MRMs). The conditions were as follows: curtain gas: 25 psi (172.38 kPa), ion spray voltage: 5.5 kV, vaporizer temperature: 600 °C, ion source gas 1: 40 psi (275.79 kPa), ion source gas 2: 60 psi (413.69 kPa), interface heater: on. Nitrogen was produced by a high purity nitrogen generator (Peak Scientific instruments Ltd., model NM20Z, Renfrewshire, Scotland) and employed as curtain, nebulizer and collision gas. Ion source and MS/MS conditions were optimized in order to achieve the optimal sensitivity by infusion of 0.2 μg⓾mL^{-1} of the derivatized NT to the mass spectrometer at the flow rate of 20 μL⓾min^{-1}. Values of mass spectrometric setting corresponded to the *m/z* (Q1/Q3) of derivatized NT. Precursor ion (Q1): 366.5, quantification ion (Q3): 120.2, confirmation ion (Q3): 106.2, declustering potential: 61 V, entrance potential: 10.5 V, collision entrance potential: 22 V, collision energies: 49 V for quantification ion and 45 V for confirmation ion, collision cell exit potential: 4 V.

4.4. Determination of NT-Pb*a* conjugate degradation by NMR spectroscopy

The sample was prepared as follows: to NT-PEG$_3$-azide[16] (12 mg, 2.2·10^{-5} mol) in CD_3OD (0.4 mL), 124 mg of TFA (1.1·10^{-3} mol, 50 equiv.) and 63 mg of acetone (50 equiv.) were added. The NMR cuvette was capped and measured over certain time. The mixture was kept at 37 °C during the experiment.

The OE bond stability of **s1** was tested after the treatment of H_2O, H_2O_2, TFA/H_2O in DMSO or MeOH solutions at RT, nevertheless, under these conditions no degradation occurred after one week of measurement (data not shown).

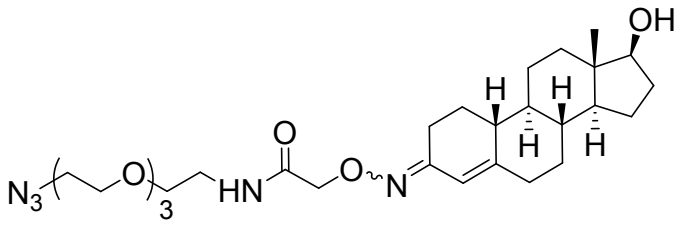

NT-PEG$_3$-azide

Fig. S28: The structure of a compound used for degradation studies

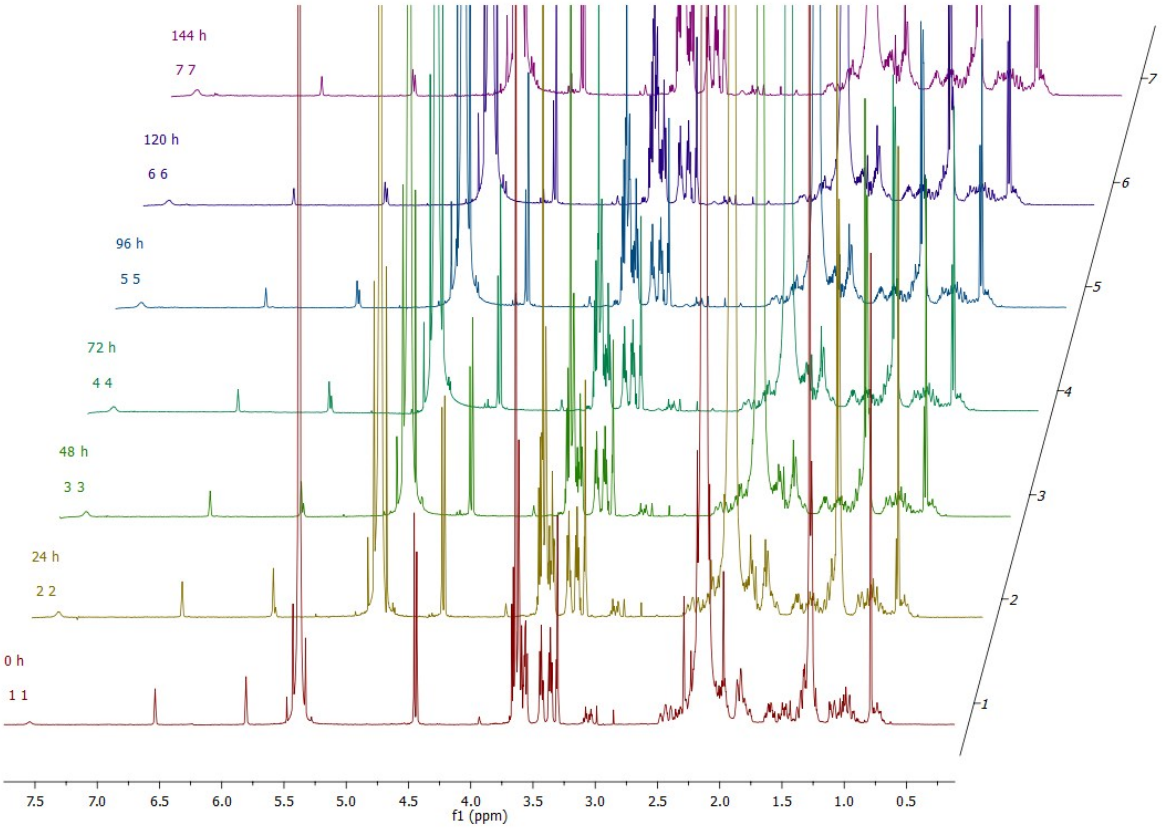

Fig. S29: Changes in NMR spectra of **s1** during 6 days of the degradation process

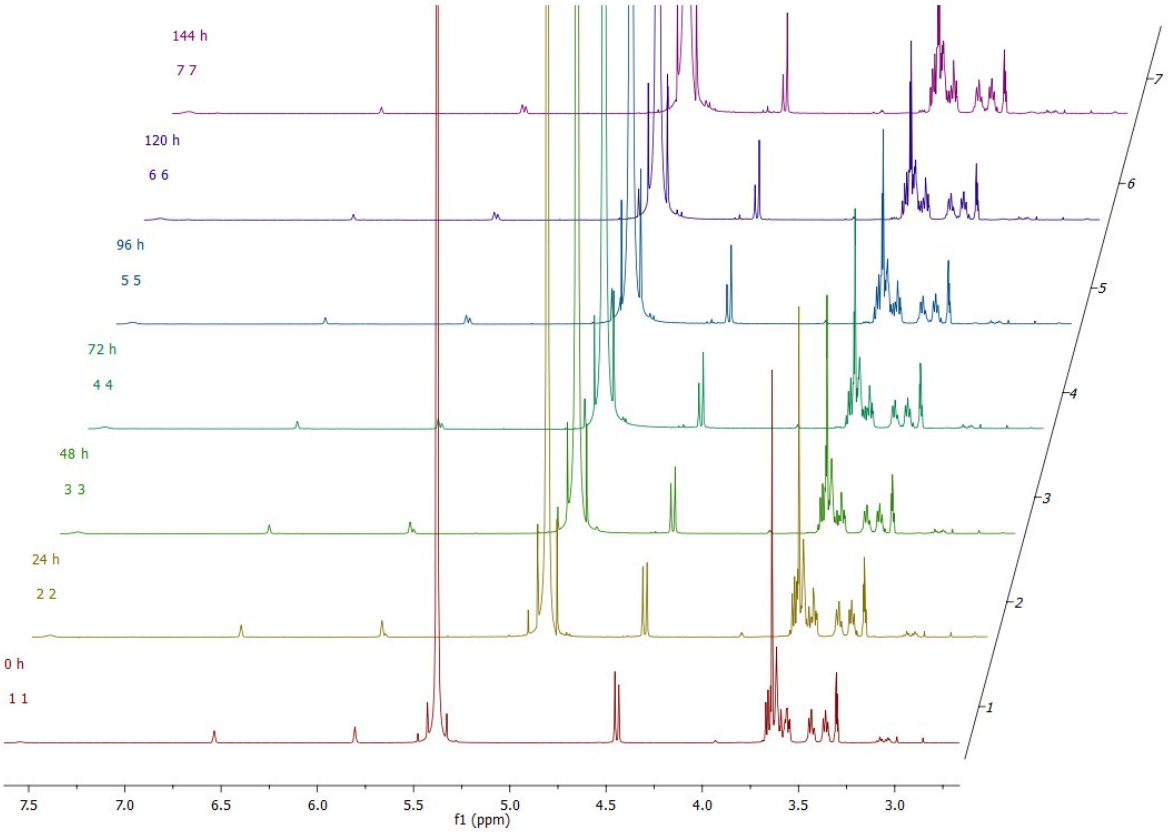

Fig. S30: Changes in NMR spectra of **s1** with a detail on the oxime doublet at 4.45 ppm

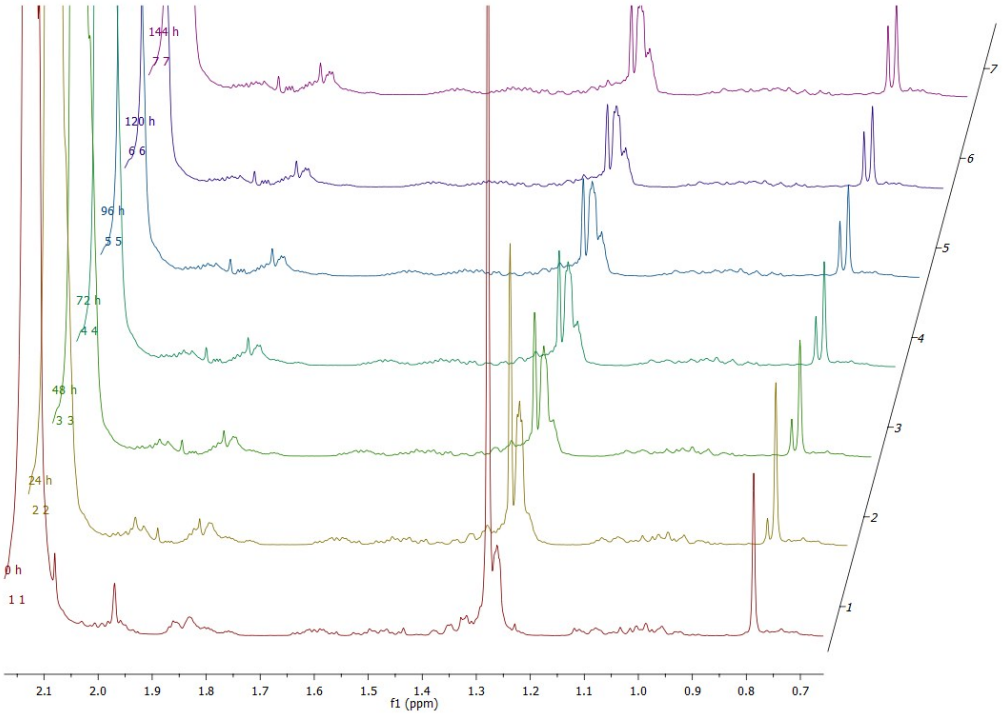

Fig. S31: Changes in NMR spectra with a detail on the steroidal cover of **s1**

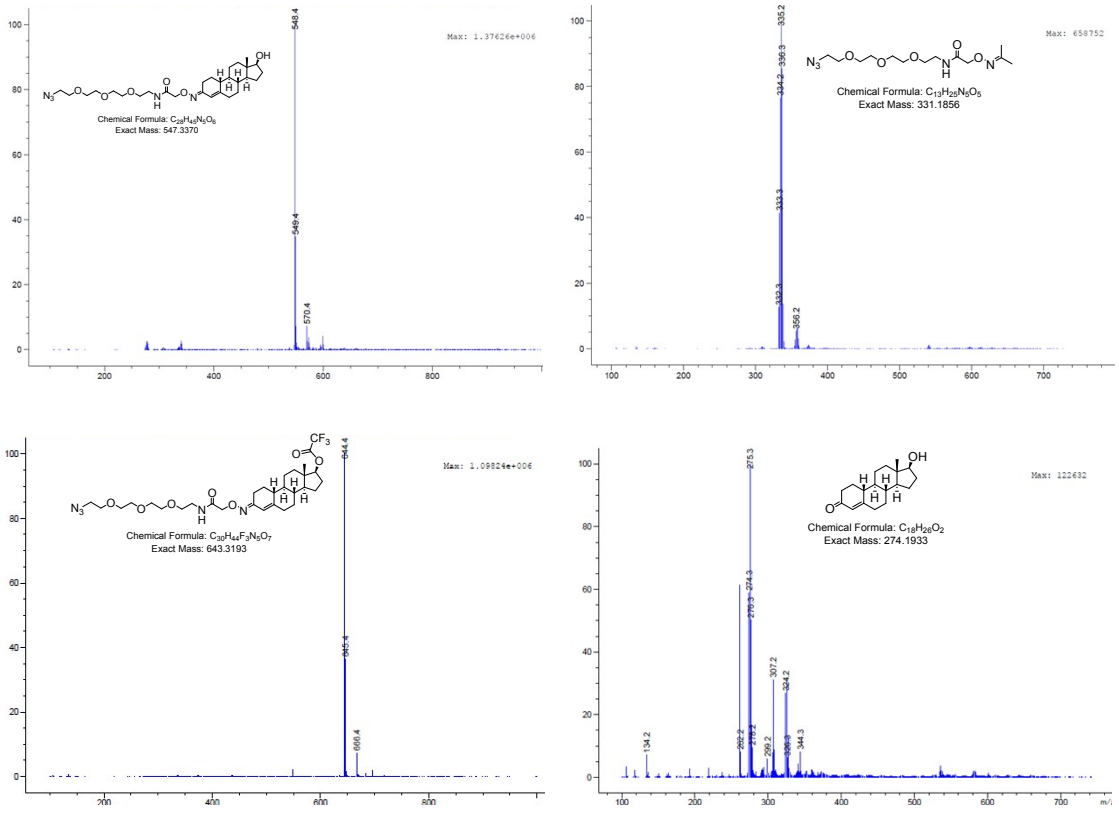

Fig. S32: LR-MS recordings of the sample used for NMR degradation study.

On reviewer´s request:

The conceptual advantage of the NT-Pb*a* conjugate is the use of a photosensitizer and the steroid activity at once. The application is based on the idea that in conjugation, the molecule better passes through the lipophilic cell membrane and in intracellular conditions, it decomposes to its original parts (pheophorbide *a* and nandrolone). Known current androgen conjugates targeting various types of cancer reported in the literature are based on a different approach than that of PDT (reviewed in Levine *et al.* (2014)[17]). Some current androgen conjugates are listed in Fig. S33.

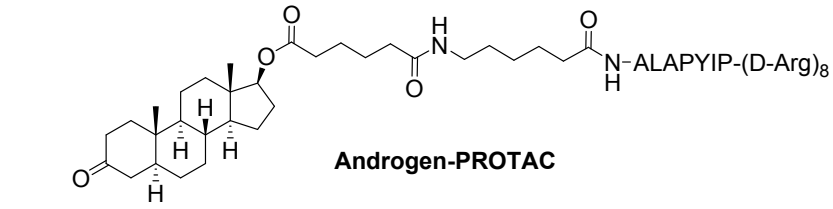

Androgen-PROTAC

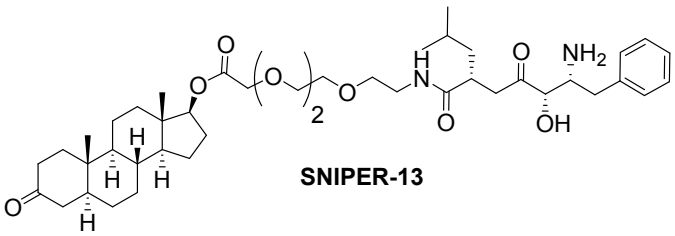

SNIPER-13

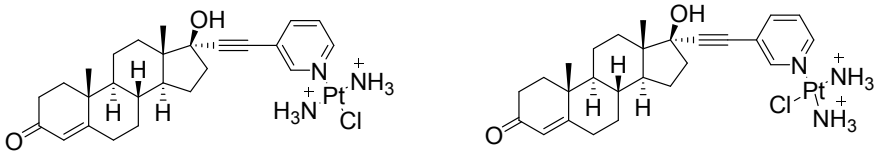

Platinum (II) androgen conjugates

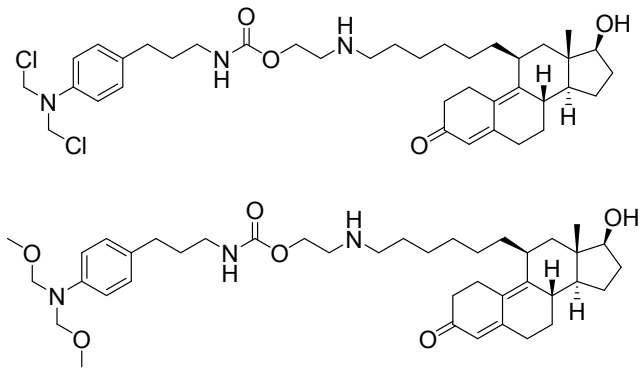

Androgen bsaed alkylating agent for targeted DNA demage

Fig. S33: Some of the currently reported steroidal androgens targeting cancer cells

Below, we provide a table (Table S3) that characterizes the NT-Pb*a* conjugate presented in our manuscript and compare it with other currently reported chlorins by their intrinsic calculated logS_0 and log*P*. However, it must be stated that the values can give just the first level of information as the solvated or moreover ionized compounds (salts) may have better bioavailability. Taken together, the lipophilicity as well as the absorbance characteristics of the NT-Pb*a* conjugate are comparable to other current chlorins. Therefore, in the terms of quality, the requirements on our novel androgen-based photosenzitizer were fulfilled.

The overall advantage of the NT-Pb*a* conjugate might be faster uptake due to the recognition of the lipophilic steroid moiety. Another advantage is the possibility to add a steroid ketone (ketoxime) of choice (targeting different steroid receptors) as well as the chlorin with a suitable functional group *via* oxime ligation.

Table S3: LogP and $LogS_0$ of current photosenzitizers from chlorin family calculated by ACD/Percepta

Photosenzitizer	**λ [nm]**	**ACD/LogP[a] GALAS[b]**	**ACD/LogP GALAS RI[c]**	**ACD/$LogS_0$[d] GALAS**	**PDT Application**	**Ref.**
NT-Pb*a*	666	7.05	0.26	-11.84	cancer cells	current work
Temoporfin (Foscan, *m*THPC)	652	5.54	0.36	-7.47	cancer	[18, 19]
Verteporfin	630	4.26	0.30	-6.99	melanoma,	[20, 21]
Photofrin (Porfimer sodium)	630	6.28	0.13	-10.66	cancer	[22, 23]
Laserphyrin (Talaporfin sodium)	664	2.76	0.28	-7.73	cancer	[22, 24]
Purlytin (Tin-ethyl-etiopurpurin; SnET2)	650	5.82	0.17	-8.88	breast cancer, psoriasis, restenosis	[25, 26]
Photochlor (HPPH)	665	6.65	0.27	-6.80	cancer	[27, 28]

[a] LogP are calculated for the parent compound, not for the salt, if applicable. Software used: ACD/Percepta 2018.1.1 (Build 3044)

[b] GALAS (Global, Adjusted Locally According to Similarity) modeling methodology according to Sazonova *et al.* (2010)[29]

[c] Reliability Index

[d] Intrinstic water solubility. $LogS_0$ are calculated for the parent compound, not for the salt, if applicable. Software: ACD/Percepta 2018.1.1 (Build 3044)

5. References

1. D. Menberu, P. V. Nguyen, K. D. Onan and P. W. Le Quesne, *J. Org. Chem.*, 1992, **57**, 2100-2104.
2. R. A. Velapoldi and H. H. Tonnesen, *J. Fluoresc.*, 2004, **14**, 465-472.
3. V. Gottfried, D. Peled, J. W. Winkelman and S. Kimel, *Photochem. Photobiol.*, 1988, **48**, 157-163.
4. R. W. Redmond and J. N. Gamlin, *Photochem. Photobiol.*, 1999, **70**, 391-475.
5. M. Jurášek, S. Rimpelová, E. Kmoníčková, P. Drašar and T. Ruml, *J. Med. Chem.*, **57**, 7947-7954.
6. V. Rapozzi, D. Ragno, A. Guerrini, C. Ferroni, E. della Pietra, D. Cesselli, G. Castoria, M. Di Donato, E. Saracino, V. Benfenati and G. Varchi, *Bioconjugate Chem.,* 2015, **26**, 1662-1671.
7. N. El-Akra, A. Noirot, J. C. Faye and J. P. Souchard, *Photochem. Photobiol. Sci.*, 2006, **5**, 996-999.
8. Y. H. Gao, V. Lovreković, A. Kussayeva, D. Y. Chen, D. Margetić and Z. L. Chen, *Eur. J. Med. Chem.*, 2019, **177**, 144-152.
9. S. S. Jalde, A. K. Chauhan, J. H. Lee, P. K. Chaturvedi, J. S. Park and Y. W. Kim, *Eur. J. Med. Chem.*, 2018, **147**, 66-76.
10. S. Srdanović, Y. H. Gao, D. Y. Chen, Y. J. Yan, D. Margetić and Z. L. Chen, *Bioorg. Med. Chem. Let.,* 2018, **28**, 1785-1791.
11. W. Zhu, Y. H. Gao, P. Y. Liao, D. Y. Chen, N. N. Sun, P. A. N. Thi, Y. J. Yan, X. F. Wu and Z. L. Chen, *Eur. J. Med. Chem.,* 2018, **160**, 146-156.
12. D. D. Xu, H. M. Lam, R. Hoeven, C. B. Xu, A. W. N. Leung and W. C. S. Cho, *Photodiagnosis Photodyn. Ther.*, 2013, **10**, 278-287.
13. T. Bříza, J. Králová, S. Rimpelová, M. Havlík, R. Kaplánek, Z. Kejik, B. Reddy, K. Záruba, T. Ruml, I. Mikula, P. Martasek, and V. Kral, *ChemPhotoChem.*, 2017, **1**, 442-450.
14. S. Rimpelová, T. Bříza, J. Králová, K. Záruba, Z. Kejík, I. Císařová, P. Martásek, T. Ruml and V. Král, *Biocon. Chem.,* 2013, **24**, 1445-1454.
15. D. Sedlak, A. Paguio and P. Bartunek, *Comb. Chem. High T. Scr.*, 2011, **14**, 248-266.

16. M. Jurasek, S. Goselova, P. Miksatkova, B. Holubova, E. Vysatova, M. Kuchar, L. Fukal, O. Lapcik and P. Drasar, *Drug Test Anal.*, 2017, **9**, 553-560.

17. P. M. Levine, M. J. Garabedian and K. Kirshenbaum, *J. Med. Chem.* 2014, **57**, 8224-8237.

18. A. E. O'Connor, W. M. Gallagher and A. T. Byrne, *Photochem. Photobiol.*, 2009, **85**, 1053-1074.

19. K. J. Lorenz and H. Maier, *Eur. Arch. Otorhinolaryngol.*, 2009, **266**, 1937-1944.

20. L. J. Scott and K. L. Goa, *Drug Aging*, 2000, **16**, 139-146.

21. D. S. Fong, *Ophthalmology*, 2000, **107**, 2314-2317.

22. J. Usuda, H. Kato, T. Okunaka, K. Furukawa, H. Tsutsui, K. Yamada, Y. Suga, H. Honda, Y. Nagatsuka, T. Ohira, M. Tsuboi and T. Hirano, *J. Thorac. Oncol.*, 2006, **1**, 489-493.

23. V. G. Schweitzer and M. L. Somers, *Lasers Surg. Med.*, 2010, **42**, 1-8.

24. J. Usuda, H. Kato, T. Okunaka, K. Furukawa, H. Honda, Y. Suga, T. Hirata, T. Ohira, M. Tsuboi and T. Hirano, *J. Clin. Oncol.*, 2006, **24**, 421s-421s.

25. L. B. Josefsen and R. W. Boyle, *Met. Based Drugs* 2008, **2008**, 276109.

26. T. S. Mang, R. Allison, G. Hewson, W. Snider and R. Moskowitz, *Cancer J. Sci. Am.*, 1998, **4**, 378-384.

27. J. Lobel, I. J. MacDonald, M. J. Ciesielski, T. Barone, W. R. Potter, J. Pollina, R. J. Plunkett, R. A. Fenstermaker and T. J. *Lasers Surg. Med.*, 2001, **29**, 397-405.

28. D. A. Bellnier, W. R. Greco, H. Nava, G. M. Loewen, A. R. Oseroff and T. J. Dougherty, *Cancer Chemother. Pharmacol.*, 2006, **57**, 40-45.

29. A. Sazonovas, P. Japertas and R. Didziapetris, *Sar Qsar Environ. Res.*, 2010, **21**, 127-148.

30. V. Rapozzi, M. Miculan and L. E. Xodo, *Cancer Biol. Ther.,* 2009, **8**, 1318-1327.

31. S. W. H. Hoi, H. M. Wong, J. Y. W. Chan, G. G. L. Yue, G. M. K. Tse, B. K. B. Law, W. P. Fong and K. P. Fung, *Phytother. Res.*, 2012, **26**, 734-742.

32. T. Gheewala, T. Skwor, G. Munirathinam, *Photodiagnosis Photodyn. Ther.* 2018, **21**, 130-137.

33. P. M. Tang, J. Y. Chan, S. W. Au, S. K. Kong, S. K. Tsui, M. M. Waye, T. C. Mak, W. P. Fong and K. P. Fung, *Cancer Biol. Ther.*, 2006, **5**, 1111-1116.